BrainPalmSeq: A curated RNA-seq database of palmitoylating and de-palmitoylating enzyme expression in the mouse brain

Authors: Wild, AR[1]; Hogg, PW[1]; Flibotte, S[2]; Nasseri, G[1]; Hollman, R[1]; Haas, K[1] and Bamji, SX[1]

Affiliations:

1 Department of Cellular and Physiological Sciences, Life Sciences Institute and Djavad Mowafaghian Centre for Brain Health, University of British Columbia

2 Life Sciences Institute Bioinformatics Facility, University of British Columbia

Correspondence:

Shernaz Bamji, Ph.D.

Department of Cellular and Physiological Sciences

Life Sciences Institute,

Djavad Mowafaghian Centre for Brain Health

University of British Columbia

2350 Health Sciences Mall

Vancouver, B.C., V6T 1Z3

Off: 604-822-4746

Abstract

Protein *S*-palmitoylation is a reversible post-translational lipid modification that plays a critical role in neuronal development and plasticity, while dysregulated *S*-palmitoylation underlies a number of severe neurological disorders. Dynamic *S*-palmitoylation is regulated by a large family of ZDHHC palmitoylating enzymes, their accessory proteins, and a small number of known de-palmitoylating enzymes. Here, we curated and analyzed expression data for the proteins that mediate *S*-palmitoylation from publicly available RNAseq datasets, providing a comprehensive overview of their distribution in the mouse nervous system. We developed a web-tool that enables interactive visualization of the expression patterns for these proteins in the nervous system (http://brainpalmseq.med.ubc.ca/), and explored this resource to find region and cell-type specific expression patterns that give insight into the function of palmitoylating and de-palmitoylating enzymes in the brain and neurological disorders. We found coordinated expression of ZDHHC enzymes with their accessory proteins, de-palmitoylating enzymes and other brain-expressed genes that included an enrichment of *S*-palmitoylation substrates. Finally, we utilized ZDHHC expression patterns to predict and validate palmitoylating enzyme-substrate interactions.

Introduction

Protein *S*-palmitoylation is a post-translational lipid modification that mediates dynamic changes in protein stability, function, and membrane localization. *S*-palmitoylation is defined as the reversible formation of a cysteine residue thioester bond with the fatty acid palmitate, and is the most prevalent post-translational lipid modification in the brain. Dynamic changes in *S*-palmitoylation are critical for neuronal development and synaptic plasticity (Fukata et al., 2013; Fukata and Fukata, 2010; Globa and Bamji, 2017; Matt et al., 2019), oligodendrocyte differentiation and myelination (Ma et al., 2021; Schneider et al., 2005), and astrocyte proliferation (Yuan et al., 2021). Furthermore, numerous neurological and psychiatric diseases have now been attributed to mutations in the genes encoding palmitoylating and de-palmitoylating enzymes, including schizophrenia, intellectual disability and CLN1 disease (Mukai et al., 2004; Nita et al., 2016; Raymond et al., 2007), underscoring the importance of proper regulation of *S*-palmitoylation for normal brain function.

S-Palmitoylation is mediated by a family of ZDHHC enzymes that share a consensus 'Asp-His-His-Cys' catalytic domain. These enzymes are structurally heterogeneous multi-pass transmembrane proteins that localize to a variety of intracellular compartments, including the Golgi apparatus, endoplasmic reticulum (ER), recycling endosomes and the plasma membrane (Globa and Bamji, 2017). The ZDHHC enzymes are known to associate with accessory proteins that regulate their stability, activity, and trafficking (Salaun et al., 2020). Several de-palmitoylating enzymes have also been identified that act as

62 the 'erasers' of *S*-palmitoylation, and are divided into three classes: the acyl-protein thioesterases that
63 shuttle between the Golgi and cytosol (APTs; Vartak et al., 2014), the predominantly lysosomal palmitoyl-
64 protein thioesterases (PPTs; Koster and Yoshii, 2019) and the more recently discovered α/β hydrolase
65 domain-containing 17 proteins (ABHD17; Lin and Conibear, 2015). Unlike other post-translational
66 modifications, palmitoylation lacks a consensus substrate amino sequence, and the mechanisms that
67 govern ZDHHC enzyme-substrate interactions are controversial, with contrasting reports of substrate
68 interactions being both promiscuous and specific (Malgapo and Linder, 2021). Currently these interactions
69 are thought to be governed by the subcellular targeting of ZDHHCs enzymes and the presence of protein-
70 protein interacting motifs within the ZDHHC N- and C-termini, which are highly diverse among the ZDHHC
71 enzymes (Rana et al., 2018). Differential gene expression can also have a profound influence on protein
72 interactions and may play a role in the coordination of *S*-palmitoylation in the brain. However, a detailed
73 overview and analysis of the precise cellular and regional expression patterns of the palmitoylating and
74 de-palmitoylating enzymes has not yet been described, and as such, little is known about how this
75 expression is coordinated in the nervous system.

76 Recent advances in single-cell RNA sequencing (scRNAseq) techniques have enabled the
77 classification of neuronal and non-neuronal cell types in unprecedented detail, providing a better
78 understanding of cellular diversity and function in the nervous system, while also providing a means to
79 study the expression patterns of individual genes across an ever-expanding range of brain regions and
80 cellular classifications. Here, we capitalized on the recent surge in RNAseq publications characterizing
81 regional and cellular transcriptomics of the mouse nervous system. We curated and analyzed expression
82 data from a number of publicly available RNAseq mouse datasets to generate a detailed analysis of the
83 expression patterns of the genes associated with *S*-palmitoylation in the mouse brain. Furthermore, we
84 present an interactive web tool that allows user-driven interrogation of the expression patterns of
85 palmitoylating and de-palmitoylating enzymes from numerous collated studies across a variety of brain
86 regions and cell types (http://brainpalmseq.med.ubc.ca/). We demonstrate the utility of this resource by
87 detailing the considerable cell type and regional heterogeneity in expression patterns of these enzyme
88 families and their accessory proteins, revealing numerous cell type enrichments and co-expression
89 patterns that allowed us to generate and test hypotheses about palmitoylating enzyme-substrate
90 interactions.

Results

BrainPalmSeq: an interactive database to search palmitoylating and depalmitoylating enzyme expression in the mouse brain

The recent development of scRNAseq has revolutionized our understanding of the complex transcriptional diversity of neuronal and non-neuronal cell types in the brain. We found however, there were several barriers to the easy access for much of this data, with no single resource available to evaluate multi-study expression data. Data can also be difficult to access when studies are not accompanied by an interactive online web viewer, while datasets that do have a web viewer employ diverse interfaces that are often complex, particularly for large scRNAseq datasets. Furthermore, the differing study specific analysis pipelines, as well as the variety of data presentation formats in web viewers including heatmaps, bar charts, tables or t-SNE plots can make datasets difficult for non-bioinformaticians to interpret and compare. In order to remove these barriers and provide easy access to expression data for the proteins that regulate *S*-palmitoylation in the brain, we created 'BrainPalmSeq', an easy-to-use web platform allowing user driven interrogation of compiled multi-study expression data at cellular resolution through simple interactive heatmaps that are populated according to user selected brain regions, cell-types or genes of interest (http://brainpalmseq.med.ubc.ca/).

To create BrainPalmSeq we first curated three large datasets from whole-brain scRNAseq studies that were acquired through selection-free cell sampling to provide high resolution expression data covering hundreds of cell types at a variety of developmental ages (Rosenberg et al., 2018; Saunders et al., 2018; Zeisel et al., 2018). As scRNAseq has several caveats including low sensitivity and high frequency of dropout events leading to incomplete detection of expressed genes (Haque et al., 2017), we complemented these datasets where possible with curation of several bulk and pooled-cell RNAseq studies that used population-level ensemble measurements from whole-brain and region-specific studies. We further included selected studies for the major glial cell types and data from the most comprehensive neuron specific study performed to date by the Allen Institute (Supplementary File 1). Together, the datasets curated in BrainPalmSeq cover all major regions of the mouse nervous system across a variety of regional and cellular resolutions.

Expression data were extracted from selected studies for the 24 mouse ZDHHC genes (*Zdhhc1-Zdhhc25*, while *Zdhhc10* is omitted), as well as the best characterized de-palmitoylating enzymes (*Ppt1*, *Lypla1*, *Lypla2*, *Abhd17a*, *Abhd17b* and *Abhd17c*) and ZDHHC accessory proteins (*Golga7*, *Golga7b* and *Selk*). Where possible, data were processed from the raw transcripts or unique molecular identifier (UMI)

122 counts using the same normalization protocol to allow for more consistent evaluation of differences in
123 gene expression within datasets. We sampled from RNAseq datasets that used a diverse range of sample
124 collection, processing and analysis techniques, allowing for direct visualization of the relative expression
125 patterns of selected genes can be directly visualized within datasets. Users can then validate their
126 observations across complimentary whole brain or region/cell-type specific datasets included in
127 BrainPalmSeq. Dropdown menus allow for selection of individual ZDHHC genes or brain regions within
128 each dataset, while the hover tool reveals metadata for each cell type, including neurotransmitter
129 designations and marker genes. We provide download links to all expression data including cell type
130 metadata so that users can replot gene expression profiles in their preferred format. To demonstrate the
131 utility of this resource, we performed a detailed exploration of selected datasets from BrainPalmSeq,
132 revealing how expression patterns can give insights into the function of the palmitoylating and de-
133 palmitoylating enzymes in the mouse brain.

134 **ZDHHC expression in the nervous system shows regional and cell-type specific patterning**

135 We began by exploring BrainPalmSeq data curated from the 'MouseBrain' dataset, which provides
136 the broadest overview of expression patterns in the nervous system (Zeisel et al., 2018). This scRNAseq
137 study sampled multiple dissected regions from the adolescent (mean age ~P25) mouse central and
138 peripheral nervous systems (CNS and PNS, respectively), identifying 265 transcriptomically unique cell-
139 types (referred to herein as metacells) for which we plotted re-normalized ZDHHC expression values,
140 according to the hierarchical cell-type clustering established by the original study (Figure 1A). While
141 ZDHHC expression was detected in all regions of the nervous system, expression of the 24 ZDHHC genes
142 was highly variable across metacell types and clusters. We measured the mean ZDHHC expression within
143 each cluster to gain insight into which cell-types in the nervous system have the greatest overall
144 expression of palmitoylating enzymes. The heatmap rows and columns were ranked (sorted by
145 descending averages) to determine which cell-types had the highest expression of ZDHHCs, and which
146 ZDHHCs were most abundantly expressed across cell-types (Figure 1B). Mean ZDHHC expression was
147 particularly high in neurons of the PNS, along with cholinergic/monoaminergic and hindbrain neurons of
148 the CNS. Of the non-neuronal metacell clusters, oligodendrocytes had the highest ZDHHC expression,
149 while other glial cell-types appear at the lower end of the ranking (Figure 1B). *Zdhhc20* was the most
150 abundantly expressed ZDHHC, with the highest mean expression across all cell-type clusters, followed by
151 *Zdhhc2*, *Zdhhc17*, *Zdhhc3* and *Zdhhc21*, while expression of *Zdhhc11*, *Zdhhc19* and *Zdhhc25* were
152 negligible. We next clustered neuronal metacells of the PNS and CNS according to the neurotransmitter
153 expression combinations, revealing the highest mean ZDHHC expression was observed in neurons that

154 utilized acetylcholine and nitric oxide as co-neurotransmitters, with cholinergic neurons featuring near
155 the top of the list in several neurotransmitter combinations (Figure 1C). Monoaminergic neurons utilizing
156 noradrenaline and serotonin also generally ranked high in the list, consistent with the data in Figure 1B
157 that ranked cholinergic and monoaminergic neurons as the metacell cluster with the highest CNS ZDHHC
158 expression overall, indicating a higher propensity for these cell-types to utilize *S*-palmitoylation as a post-
159 translational mechanism to modify cellular signaling. We performed comparative analysis of ZDHHC
160 expression on another large-scale scRNAseq study of the mouse brain that sampled a variety of cortical
161 and subcortical structures of the adult mouse (P60-P70) (Saunders et al., 2018; 'DropViz'; Figure 1-figure
162 supplement 1A). We found expression patterns and enrichments to be similar across these two
163 independent, large scale scRNAseq studies, supporting the general trends observed within the
164 MouseBrain dataset.

165 To gain insight into the potential networks of ZDHHC enzymes that might work together to coordinate
166 *S*-palmitoylation in different cell types we performed co-expression analysis (Spearman correlation)
167 between ZDHHC genes across all 265 metacell types in the MouseBrain dataset (Figure 1D). Neuron
168 enriched *Zdhhc3*, *Zdhhc8*, *Zdhhc17* and *Zdhhc21* formed the strongest network of co-expression
169 associations, while glial cell enriched *Zdhhc2, Zdhhc9* and *Zdhhc20* formed less robust correlations with
170 other ZDHHCs. Weaker correlations were observed across the 565 cell-types in the DropViz dataset, which
171 may reflect the absence of the PNS neurons and glia in this study (Figure 1-figure supplement 1D).

172 In order to create a list of potential substrates for the ZDHHCs in the mouse nervous system, we
173 expanded our co-expression analysis to include all expressed genes from the 'MouseBrain' dataset that
174 had significant correlation ($R > 0.7$) with one or more ZDHHC. We identified 914 genes with expression
175 patterns that were significantly correlated with ZDHHCs. This list was cross-referenced with the mouse
176 SwissPalm database of *S*-palmitoylated substrates identified in at least one palmitoyl-proteome or
177 experimentally validated (SwissPalm annotated; Blanc et al., 2015, 2019). We found that genes that
178 showed correlated expression with a ZDHHC were significantly enriched with *S*-palmitoylation substrates,
179 indicating that ZDHHCs are more likely to be co-expressed with their *S*-palmitoylation substrates in the
180 brain (Figure 1E). Co-expression analysis of the 'DropViz' dataset revealed a similar enrichment of *S*-
181 palmitoylation substrates that were co-expressed with ZDHHCs (Figure 1-figure supplement 1E),
182 supporting the notion of ZDHHC enzyme-substrate co-expression. PANTHER GO analysis of the ZDHHC co-
183 expressed *S*-palmitoylation substrates curated from 'MouseBrain' revealed several significant
184 enrichments in GO terms for biological processes related to protein localization (Figure 1F). These findings

185 are consistent with the known role of *S*-palmitoylation in regulating protein localization and signaling
186 complexes at cellular membranes.

187 **Heterogeneity in ZDHHC expression within excitatory neurons of the dorsal hippocampus**

188 The hippocampus is a heavily studied brain region that is critical for learning and memory (Bird
189 and Burgess, 2008). A recent pooled-cell RNAseq study of excitatory neurons in the hippocampus revealed
190 extensive regional variability in gene expression profiles of the hippocampal tri-synaptic loop
191 (hipposeq.janelia.org; Cembrowski et al., 2016). In order to clearly visualize if ZDHHC expression also
192 varied within these different cell populations, we projected log transformed expression heatmaps
193 generated in BrainPalmSeq for the 'hipposeq' dorsal-ventral excitatory neuron dataset on to anatomical
194 maps of the dorsal hippocampus (Figure 2A). We observed considerable heterogeneity in the regional
195 expression patterns of the ZDHHCs in the hippocampus. Hierarchical clustering analysis revealed that the
196 ZDHHCs could be grouped into those that showed similar expression in all regions, those that were
197 dentate gyrus granule cell (DG) enriched, DG depleted or CA1/CA2 enriched (Figure 2B). We generated
198 comparative heatmaps for several scRNAseq studies curated in BrainPalmSeq that also quantified the
199 hippocampal excitatory neuron transcriptome and found similar cross-study expression patterns for many
200 of the ZDHHCs (Figure 2-figure supplement 1A). Furthermore, *in situ* hybridization data from the Allen
201 Institute showed a high degree of overlap with the 'hipposeq' derived ZDHHC expression patterns,
202 supporting the replicability of the expression patterns observed in the 'hipposeq' dataset (Figure 2-figure
203 supplement 1B; Supplementary File 2).

204 We next sought to utilize the 'hipposeq' dataset to determine if there might be regional
205 differences in the expression of *S*-palmitoylation substrates in excitatory neurons of the dorsal
206 hippocampus, which may be potential substrates for regionally enriched ZDHHC enzymes. To investigate
207 the regionally enriched predicted hippocampal palmitoylome, we utilized the enrichment analysis tools
208 built in to hipposeq.janelia.org (see Materials and Methods). Neurons in each hippocampal sub-region
209 expressed unique *S*-palmitoylation substrates that were related to highly divergent functions. We found
210 for CA1 neurons, which have the highest expression of *Zdhhc2*, *Zdhhc17*, *Zdhhc23* and *Zdhhc9* (Figure 2C),
211 the CA1 enriched predicted palmitoylome (Figure 2D) generated KEGG pathways related to 'Calcium
212 signaling', 'Glutamatergic synapse' and 'Long term potentiation', supporting the known role for *S*-
213 palmitoylation in CA1 hippocampal synaptic plasticity (Figure 2E; Ji and Skup, 2021; Matt et al., 2019). The
214 CA1 predicted palmitoylome was composed of around 46 % synaptic proteins (SynGO annotated), with
215 SynGO ontologies related to 'synaptic vesicle exocytosis' and 'synapse organization' (Figure 2F; Koopmans

216 et al., 2019). In contrast, the predicted palmitoylome of DG granule cells which have the highest
217 expression of *Zdhhc21*, *Zdhhc4*, *Zdhhc24* and *Zdhhc8* (Figure 2G, H) generated KEGG pathways related to
218 'Ribosome', 'Cholinergic synapse' and 'Parkinson's disease' (Figure 2I). The DG predicted-palmitoylome
219 was composed of 29 % synaptic proteins (SynGO annotated), with SynGO ontologies related to 'protein
220 translation at presynapse' and 'protein translation at postsynapse', revealing a potential role for
221 palmitoylating enzymes in regulating translation in this cell-type that has not yet been studied (Figure 2J).
222 Together, we have described patterns of restricted expression of ZDHHC enzymes and *S*-palmitoylation
223 substrates in the dorsal mouse hippocampus, and generated regionally-enriched predicted-
224 palmitoylomes that provide insight into the role of *S*-palmitoylation in neuronal function in each of these
225 hippocampal sub-regions.

226 **Neocortical ZDHHC expression is partially segregated across cortical layers and neuronal subclasses**

227 We next examined scRNAseq datasets curated in BrainPalmSeq from the cortex, beginning with a
228 study of the primary somatosensory cortex (SSp; Zeisel et al., 2015). We projected heatmaps of pyramidal
229 excitatory neuron ZDHHC expression generated in BrainPalmSeq onto cortical layer diagrams of SSp, again
230 revealing anatomically heterogeneous excitatory neuron expression patterns for several of the ZDHHC
231 transcripts. Clustering primarily grouped the enzymes according to expression levels, with *Zdhhc21*,
232 *Zdhhc17* and *Zdhhc8* displaying the highest relative expression (Figure 3B). *Zdhhc2*, *Zdhhc3* and *Zdhhc20*
233 expression was also high, with the remainder of the ZDHHCs having moderate to low expression. We
234 compared these expression patterns with other datasets curated in BrainPalmSeq (Figure 3-figure
235 supplement 1A), which revealed many consistent patterns of expression maintained across several
236 independent studies. For example, multiple studies reported high expression of *Zdhhc8* in cortical Layer
237 2/3, enrichment of *Zdhhc2* in Layer 4 and elevated expression of *Zdhhc21* in all layers, particularly in Layer
238 5. *Zdhhc3* and *Zdhhc20* were also broadly expressed in all cortical layers across studies. Similar patterns
239 were seen in the SSp region from available in situ hybridization studies from Allen Brain Institute (Figure
240 3-figure supplement 1B).

241 We examined expression patterns of the ZDHHC enzymes from one of the largest neuronal
242 scRNAseq studies from the isocortex performed by the Allen Brain Institute, which identified 236
243 glutamatergic and 117 GABAergic distinct neuron metacell types (Yao et al., 2021). We averaged ZDHHC
244 expression data downloaded from BrainPalmSeq for the major metacell clusters from all regions of the
245 isocortex, according to their anatomical location and/or axon projection and plotted ranked heatmaps
246 (Figure 3C,D). We again found that *Zdhhc20* was the ZDHHC transcript with the highest expression, with

247 broad expression across the majority of glutamatergic and GABAergic cell-types. Elevated expression of
248 *Zdhhc14* was found in both glutamatergic and GABAergic neurons, which was moderately expressed in
249 other studies of the brain and cortex discussed previously. Numerous subtypes of projection neurons
250 featured at the top of the ranking including pyramidal tract (PT) projecting neurons found in layer 5 of the
251 cortex, that have extensive dendritic branching and long-range axonal projections to the spinal cord,
252 brainstem and midbrain, as well as the ipsilateral cortex, striatum and thalamus. Other neuron subtypes
253 with high ZDHHC expression included a number of intratelencephalic (IT) projecting neuron classes,
254 including those from Layer 4/5 of the temporal/perirhinal/ectorhinal/entorhinal cortices, Car3 expressing
255 Layer 6 neurons, Layer 6b neurons, and Cortex IT projecting neurons from all cortical layers (Harris and
256 Shepherd, 2015; Yao et al., 2021). GABAergic neurons of the isocortex also showed elevated expression
257 of the common neuronal ZDHHCs including *Zdhhc2*, *Zdhhc3*, *Zdhhc14*, *Zdhhc17*, *Zdhhc20* and *Zdhhc21*.
258 The highest mean ranked expression was observed in the recently categorized Sncg neurons that
259 correspond to *Vip*$^+$/*Cck*$^+$ multipolar or basket cells (Tasic et al., 2018), and lowest expression was observed
260 in the Vip subclass of interneurons.

261 Together, our observations reveal that the complex transcriptional diversity of neurons that has
262 recently been revealed by RNA sequencing also includes heterogeneity in the expression of the ZDHHC
263 enzymes that mediate palmitoylation. These expression patterns are likely to influence enzyme-substrate
264 interactions along with the function of *S*-palmitoylation substrates, and thus influence neuronal
265 development, function and synaptic plasticity.

266 **De-palmitoylating enzyme and ZDHHC accessory protein expression in the nervous system shows**
267 **regional and cell-type specific patterning**

268 Dynamic turnover of protein *S*-palmitoylation is mediated by the activity of de-palmitoylating
269 enzymes, which determine the half-life of *S*-palmitoylation on a target protein. These include acyl-protein
270 thioesterases 1 and 2 (APT1, APT2; encoded by *Lypla1*, *Lypla2*), palmitoyl-protein thioesterase 1 (PPT1)
271 and the more recently identified α/β hydrolase domain-containing 17 proteins (ABHD17A, ABHD17B and
272 ABHD17C). Compared with the ZDHHC enzymes, relatively less is known about the substrates, sub-cellular
273 localization and brain expression patterns of this family of enzymes. We next explored BrainPalmSeq to
274 determine which cell-types/brain regions show the highest expression of de-palmitoylating enzymes.

275 We first examined expression heatmaps for the known de-palmitoylating enzymes across the 265
276 cell-types identified in the 'MouseBrain' dataset (Figure 4A) and the cell-type averages for the 565 cell-
277 types from the 'DropViz' dataset (Figure 4-figure supplement 1A). *Ppt1* and *Abhd17a* were the enzymes

278 with the broadest expression across all cell-types, with *Ppt1* expression being notably elevated in neurons
279 of the hindbrain and immune cells, and *Abhd17a* being elevated in hindbrain neurons, sensory neurons,
280 oligodendrocytes and epithelial cells. Ranked expression (sorted by descending averages) of de-
281 palmitoylating enzymes in the 'MouseBrain' (Figure 4B) and 'DropViz' (Figure 4-figure supplement 1B)
282 datasets classified oligodendrocyte lineage cells among the cell-types with the highest expression of de-
283 palmitoylating enzymes overall, primarily due to elevated expression of *Abhd17b*. This mirrors
284 oligodendrocyte enrichment of ZDHHC enzyme expression, again indicating that dynamic regulation of *S*-
285 palmitoylation may be particularly important in this cell type. *Lypla2* expression was greater than *Lypla1*
286 overall in the brain, with *Lypla2* expression being highest in neurons and ependymal cells (Figure 4-figure
287 supplement 1A). *Abhd17c* had the lowest brain expression of all the de-palmitoylating enzymes studied.
288 Correlation analysis between the ZDHHCs and de-palmitoylating enzymes revealed numerous instances
289 of co-expression with almost every ZDHHC (Figure 4D), revealing potential cooperative pairs of
290 palmitoylating and de-palmitoylating enzymes in the nervous system.

291 Although the ZDHHC enzymes are thought to act autonomously, several accessory proteins have
292 been discovered that can regulate ZDHHC stability, localization and catalytic activity (Salaun et al., 2020).
293 These include GOLGA7 (GCP16), which can bind to ZDHHC9 and enhance both protein stability and
294 enzymatic activity by stabilizing the ZDHHC9 auto-palmitoylated intermediate that is formed prior to
295 palmitate transfer from the enzyme to the substrate protein (Mitchell et al., 2014; Swarthout et al., 2005).
296 Both GOLGA7 and related isoform GOLGA7B are also able to interact with ZDHHC5, with the latter
297 influencing ZDHHC5 plasma membrane localization (Woodley and Collins, 2019). Finally, SELK (SELENOK;
298 Selenoprotein K) is an ER localized protein that was found to interact with ZDHHC6, stabilize the auto-
299 palmitoylated intermediate and increase palmitoylation of substrate proteins including the IP_3 receptor
300 (Fredericks et al., 2017, 2014). We observed widespread expression of *Selk* across all cell-types, with
301 expression being considerably higher than any of the ZDHHCs, de-palmitoylating enzymes or other
302 accessory proteins (Figure 4A, S4A). This is consistent with the known functions of SELK in the ER
303 associated protein degradation pathway and regulation of ER calcium flux (Pitts and Hoffmann, 2018).
304 *Golga7b* expression was widespread across neuronal subtypes but barely detected in glial cells (Figure 4A,
305 S4A). Accordingly, *Golga7b* expression was also strongly correlated with several of the ZDHHCs that were
306 most highly expressed in neurons, including *Zdhhc3*, *Zdhhc8*, *Zdhhc17* and *Zdhhc21* (Figure 4D). In
307 contrast, *Golga7* was enriched in glial cells, particularly in oligodendrocytes, similar to ZDHHC9 for which
308 GOLGA7 is a key accessory protein (Figure 4A, S4A). GOLGA7 and GOLGA7B share 61% amino acid

309 similarity, but their expression was either not correlated or was negatively correlated, indicating that the
310 ZDHHC association of each of these proteins may be regulated in part by differential expression.

311 **Loss of function mutations in palmitoylating and de-palmitoylating enzymes**

312 Impaired regulation of *S*-palmitoylation has been implicated in numerous neurological disorders,
313 many of which are due to loss of function (LOF) mutations in the genes encoding palmitoylating and de-
314 palmitoylating enzymes (Cho and Park, 2016; Matt et al., 2019). We next sought to determine if the
315 regional and cell type expression data available in BrainPalmSeq could reveal insights into the
316 pathogenesis of disorders caused by LOF mutations in palmitoylating and de-palmitoylating enzymes. As
317 many of these diseases have a neurodevelopmental origin, we examined whole brain datasets curated in
318 BrainPalmSeq from the neonatal (Rosenberg et al., 2018), adolescent (Zeisel et al., 2018) and adult
319 (Sjöstedt et al., 2020) mouse brain.

320 A single nucleotide polymorphism (SNP) in the *ZDHHC8* gene has been implicated in increased
321 susceptibility to schizophrenia (Chen et al., 2004; Mukai et al., 2004), while hemizygous microdeletion in
322 the chromosomal locus 22q11, which encodes a number of genes including *ZDHHC8*, is one of the highest
323 known genetic risk factors to developing schizophrenia (Figure 5A; Karayiorgou et al., 2010). To assess the
324 developmental expression of *Zdhhc8*, we averaged expression within broadly defined cell-type clusters
325 that could be applied to both the Rosenberg and Zeisel scRNAseq datasets (Figure 5A, B; Supplementary
326 File 3). *Zdhhc8* expression was highest in neurons of the cortex and hippocampus, followed by neurons of
327 the mid- and hindbrain at both developmental ages. To explore regional expression in the adult mouse
328 brain, we projected BrainPalmSeq generated heatmaps expression data from the 'Protein Atlas' mouse
329 whole brain dataset (bulk RNAseq from major brain regions; Figure 5-figure supplement 1) onto
330 anatomical maps of the mouse brain, again revealing highest expression of *Zdhhc8* in the cortex, followed
331 by the hippocampus and basal ganglia (Figure 5C; Sjöstedt et al., 2020). *Zdhhc8* expression was particularly
332 enriched in Layer 2/3 of the neonatal (not shown) and adult mouse (Figure S3B) cortex, which is the
333 cortical layer with the most pronounced morphological deficits in patients with Schizophrenia (Glantz and
334 Lewis, 2000; Kolluri et al., 2005; Wagstyl et al., 2016). Together, we found *Zdhhc8* expression patterns in
335 the mouse brain that are established early in postnatal development and maintained into adulthood, that
336 also overlay with many brain regions and cell types that are known to be severely affected in patients with
337 schizophrenia. These observations support a model in which LOF *ZDHHC8* mutations may elicit many of
338 the symptoms of schizophrenia by disrupting *S*-palmitoylation and normal neuronal development in these
339 brain regions.

340 Mutations in the *ZDHHC9* gene, which is located on the X chromosome, have been identified in
341 ~2% of individuals with X-linked intellectual disability (ID) (Raymond et al., 2007; Tzschach et al., 2015).
342 Neuroanatomical abnormalities reported in patients with *ZDHHC9* mutations include decreased cortical,
343 thalamic and striatal volume, as well as widespread white matter abnormalities with prominent
344 hypoplasia (under-development) of the corpus callosum (Baker et al., 2015; Bathelt et al., 2016).
345 Disrupted white matter integrity is thought to underlie deficits in global and local brain connectivity in
346 patients with *ZDHHC9* mutations (Bathelt et al., 2017). *Zdhhc9* knock-out mice also develop similar
347 pathological changes, including decreased volume of the corpus callosum (Kouskou et al., 2018). We
348 observed considerable cell-type enrichment of *Zdhhc9* in oligodendrocytes across studies and
349 developmental ages (Figure 5D, E), accompanied by moderate neuronal expression of *Zdhhc9* relative to
350 other ZDHHCs across several brain regions including the hippocampus and cortex (Figure 2A, 3A, 5D, E),
351 consistent with the known function of ZDHHC9 in regulating neuronal development (Shimell et al., 2019).
352 Regionally, we found *Zdhhc9* expression in adult mice to be highly enriched in the corpus callosum, the
353 largest white matter tract in the brain (Figure 5F). As myelin production by oligodendrocytes is critical for
354 maintaining white matter integrity, these observations indicate that disrupting *S*-palmitoylation in
355 oligodendrocytes may underlie the white matter pathology and decreased connectivity observed in
356 patients with X-linked ID and *ZDHHC9* mutations.

357 Infantile neuronal ceroid lipofuscinosis (INCL or CLN1 disease) is a severe neurological disorder
358 caused by LOF mutations in the *PPT1* gene that presents in the first 6 - 12 months of life and is
359 characterized by rapid developmental regression, blindness and seizures, with continual deterioration
360 until death in early childhood (Nita et al., 2016). While PPT1 is thought to primarily localize to lysosomes
361 with an essential role in lysosomal degradation of *S*-palmitoylated proteins (Lu et al., 1996), this protein
362 also has a synapse-specific function in regulating synaptic vesicle cycling and synaptic transmission (Koster
363 and Yoshii, 2019). We found that neuronal *Ppt1* expression was high in postnatal neurons of the spinal
364 cord, olfactory bulb and mid/hindbrain, while microglia were the highest expressing non-neuronal cell
365 type at both postnatal ages (Figure 5G, H). Neurodegeneration has been detected in the spinal cord prior
366 to onset within the brain in *Ppt1* knock-out mice, accompanied by extensive glial cell activation including
367 microgliosis, which is a pathological hallmark of CLN1 disease (Shyng et al., 2017). Mid-/hindbrain neurons
368 also had high expression of *Ppt1,* consistent with reports that *Ppt1* knock-out mice show early signs of
369 brain pathology in the thalamus (Kielar et al., 2007). Overall, we observed widespread *Ppt1* expression in
370 almost every brain region in adult mice, consistent with the sweeping neurological deficits associated with

371 CLN1 disease (Figure 5I). Together, these observations reveal how the loss of *Ppt1* in cell types with high
372 *Ppt1* expression may lead to cell death/dysfuntion in the early stages of CLN1 disease.

373 **ZDHHC cell type enrichments can be used to predict and validate ZDHHC substrates**

374 We next tested if ZDHHC expression patterns identified from BrainPalmSeq could be used to
375 predict and validate *S*-palmitoylation substrates for regionally enriched ZDHHCs. We focused on *Zdhhc9*,
376 which showed a consistent cell-type enrichment in oligodendrocytes across multiple studies in
377 BrainPalmSeq, while LOF mutations in *ZDHHC9* are known to result in reduced white matter integrity in
378 the brain (Raymond et al., 2007). Examination of the Marques et al oligodendrocyte-specific scRNAseq
379 dataset curated in BrainPalmSeq revealed that oligodendrocyte *Zdhhc9* expression increased throughout
380 maturation, with highest expression in the myelin forming (MFOL) intermediate-maturity subtype of
381 oligodendrocytes, while slightly lower expression is maintained in mature oligodendrocytes (MOL; Figure
382 6A; Marques et al., 2016).

383 To identify potential substrates for ZDHHC9, we cross-referenced a list of MFOL/MOL enriched genes
384 identified in the study by Marques et al (Marques et al., 2016) with the SwissPalm database to identify
385 known palmitoylation substrates in these cell types (Swiss Palm Annotated; Figure 6B; Blanc et al., 2019,
386 2015). PANTHER analysis of cellular component enrichments for these substrates revealed the most
387 significant enrichment was for the term 'myelin sheath' (30 proteins; Figure 6C, Figure 6-figure
388 supplement 1). To determine if any of the myelin sheath associated proteins could be palmitoylated by
389 ZDHHC9, we selected three proteins (MOBP, PLP1 and CNP) for experimental validation (Figure 6C). We
390 separately expressed each of these candidate substrates together with ZDHHC9 and its accessory protein
391 GOLGA7 in HEK293T cells, and determined the proportion of palmitoylated substrate using an acyl-resin
392 assisted capture (acyl-RAC) palmitoylation assay (Forrester et al., 2011). In this assay, free cysteine
393 residues of cell lysates were first blocked, followed by cleavage of the palmitoyl-thioester bond with
394 hydroxylamine, resulting in the exposure of a free sulfhydryl group. Cleaved lysates were then applied to
395 a Sepharose resin to capture palmitoylated proteins containing a free sulfhydryl group. Un-bound proteins
396 (Unpalm Fraction) were first extracted from the resin mixture, followed by elution of bound palmitoylated
397 proteins from the resin (Palm Fraction). To assess non-specific binding of unpalmitoylated protein to the
398 resin, half of the cell lysate was processed without the cleavage step (NSB control). Co-expression of HA-
399 ZDHHC9 and FLAG-GOLGA7 increased the palmitoylated fraction of MOBP and PLP1, indicating that these
400 proteins are substrates for ZDHHC9 (Figure 6D, E, G). Conversely, CNP was not identified as a ZDHHC9
401 substrate in our assay (Figure 6F, G). These results demonstrate how the cell-type enrichments of ZDHHC

402 enzymes identified in this study can be used, along with the lists of similarly enriched palmitoylation
403 substrates, to guide the identification of enzyme-substrate interactions that can be further investigated
404 *in vivo*.

405 **Discussion**

406 **BrainPalmSeq as a tool to generate hypotheses about proteins that control S-palmitoylation in the**
407 **brain**

408 We have demonstrated the utility of BrainPalmSeq by providing examples of how this database
409 can be used to explore detailed region and cell type-specific expression patterns of the known
410 palmitoylating and de-palmitoylating enzymes, and their accessory proteins. We reveal how these
411 expression patterns can be used to predict/validate *S*-palmitoylation substrates and better understand
412 diseases associated with loss of function mutations in the enzymes that mediate *S*-palmitoylation. Given
413 the number of brain regions and cell types incorporated into BrainPalmSeq that were not discussed in the
414 present study, including the thalamus, hypothalamus, amygdala, striatum and cerebellum, there is rich
415 potential for users to explore the data and generate hypotheses about the role of these enzymes in the
416 brain.

417 **Insights into the role of *S*-palmitoylation associated enzymes in brain physiology and pathology**

418 While we found that many of the proteins we studied showed correlated expression across the
419 entire mouse nervous system, particularly those enriched in neurons including *Zdhhc3*, *Zdhhc8*, *Zdhhc17*
420 and *Zdhhc21*, expression of these genes was segregated within more narrowly defined neuronal
421 populations such as the excitatory pyramidal neurons within the hippocampal tri-synaptic loop or layers
422 of the somatosensory cortex. This is in line with the extensive neuronal transcriptional heterogeneity
423 identified recently by a number of scRNAseq studies (Saunders et al., 2018; Yao et al., 2021; Zeisel et al.,
424 2015, 2018). The genes that determine neuronal identity fall under four broad functional categories: those
425 that control transcriptional programs, membrane conductance, neurotransmission, or synaptic
426 connectivity (Zeisel et al., 2018). We also report heterogeneity in the neuronal fingerprint of
427 palmitoylating and de-palmitoylating enzyme expression, which will in turn give rise to differential *S*-
428 palmitoylation of neuronal proteins. Future work is needed to determine how these specific ZDHHC
429 expression patterns are related to dynamic *S*-palmitoylation in these neuronal sub-types, and how the
430 elevated expression of certain ZDHHCs can alter neuronal function. Given that *S*-palmitoylation is a key
431 regulator of neuronal development, and that nearly half of all known synaptic proteins are substrates for

432 palmitoylation (Sanders et al., 2015), this heterogeneity is likely to be a key mechanism in the fine tuning
433 of neuronal function and synaptic transmission.

434 Many of the ZDHHCs that we observed with consistently elevated expression across multiple
435 studies in BrainPalmSeq have already been studied in the context of neuronal signaling, including ZDHHC2,
436 ZDHHC3, ZDHHC8 and ZDHHC17 (Ji and Skup, 2021; Matt et al., 2019). In contrast, ZDHHC20 and ZDHHC21
437 are relatively understudied in the nervous system, despite our observation that these are two of the most
438 abundantly expressed ZDHHCs across neuronal cell types, with broad expression of *Zdhhc20* also in glial
439 cells. A recent study defined a role for ZDHHC21 in the palmitoylation of serotonergic receptor 5-HT1A
440 and implicated downregulation of ZDHHC21 in the development of major depressive disorder (Gorinski et
441 al., 2019). Interestingly, both ZDHHC20 and ZDHHC21 have a potential role in the pathogenesis of
442 Alzheimer's disease, as they can palmitoylate BACE1, Tau and amyloid precursor protein (Cho and Park,
443 2016). Further work is required to understand the likely important role of these enzymes in the brain.

444 We made several other interesting observations during our examination of BrainPalmSeq that
445 were not discussed in detail in the present study but we believe warrant further investigation. For
446 example, the particularly elevated expression of *Zdhhc2* in peripheral sensory neurons may indicate an
447 important role for palmitoylation in this cell type. Across multiple studies we observed striking enrichment
448 of *Zdhhc14* in cerebellar Purkinje neurons, a cell type in which *S*-palmitoylation is known to be important
449 for long-term depression, although the role of ZDHHC14 in this process has not yet been investigated
450 (Thomas et al., 2013). *Zdhhc23* was similarly enriched in the CA2 region of the hippocampus, with
451 comparatively low expression across other cell types. More broadly, the elevated expression of a variety
452 of palmitoylating enzymes in neurons that utilize acetylcholine or monoamines as neurotransmitters
453 would suggest an important role for *S*-palmitoylation in these neurons that has yet to be explored.
454 Accordingly, many of the key proteins involved in cholinergic synaptic transmission are *S*-palmitoylation
455 substrates including muscarinic acetylcholine receptor M2 (CHRM2), acetylcholinesterase (ACHE) and
456 ATP-citrate synthase (ACLY; Blanc et al., 2015, 2019). Our observations of co-enrichment of certain
457 palmitoylating and de-palmitoylating enzymes are also of interest, such as *Abhd17b* and *Zdhhc9* in
458 oligodendrocytes. It is possible that these enzymes share substrates to mediate dynamic
459 palmitoylation/de-palmitoylation, or conversely, have separate substrates in order to maintain stable *S*-
460 palmitoylation states of certain oligodendrocyte expressed proteins. Importantly, the data accessibility in
461 BrainPalmSeq will enable researchers to develop hypotheses regarding their cell type, brain region or
462 protein of interest.

463 The palmitoylome of each cell type in the nervous system is likely to be highly heterogeneous and
464 will be determined by the expression of both the *S*-palmitoylation substrates and the palmitoylating and
465 de-palmitoylating enzymes in a given cell type. Furthermore, accumulating evidence has revealed that
466 this palmitoylome can be altered by extrinsic factors such as chronic stress and neuronal activity (Kang et
467 al., 2008; Zareba-Koziol et al., 2019). While we have provided predicted palmitoylomes composed of
468 several highly expressed or enriched *S*-palmitoylation substrates in select brain regions and cell types,
469 experimental validation to reveal the relative palmitoylation of substrates under various conditions is
470 needed to fully understand these cellular differences. Nevertheless, we were able utilize our predicted
471 palmitoylomes to validate substrates for ZDHHC9, providing insight into the potential role of this enzyme
472 in myelin regulation in the brain.

473 Neurological disorders that arise from LOF gene mutations may be predicted to lead to
474 pathological changes that are more severe in the brain regions in which these genes are most highly
475 expressed. We observed this type of regional overlay for the expression patterns of *Zdhhc8*, *Zdhhc9* and
476 *Ppt1*. Numerous other brain disorders are thought to be exacerbated by an imbalance in *S*-palmitoylation,
477 such as decreased *S*-palmitoylation of HTT in Huntington's disease (Virlogeux et al., 2021; Yanai et al.,
478 2006), increased *S*-palmitoylation of APP and TAU in Alzheimer's disease (Cho and Park, 2016), and
479 reduced *S*-palmitoylation of 5-HTA receptor in major depressive disorder (Gorinski et al., 2019). Efforts
480 are already underway to normalize aberrant *S*-palmitoylation in neurological diseases in order to improve
481 clinical outcomes (Roberts et al., 2012; Virlogeux et al., 2021). Understanding the brain expression
482 patterns of the enzymes that mediate palmitoylation in these diseases will be paramount to developing
483 and targeting such therapeutics.

484 **Differential gene expression as a means to control *S*-palmitoylation in the brain**

485 The mechanisms that govern ZDHHC enzyme-substrate interactions are complex and still not fully
486 understood. While the majority of post-translational modifications including phosphorylation and N-
487 glycosylation are highly sequence specific (Schwarz and Aebi, 2011; Ubersax and Ferrell, 2007), several
488 studies have revealed that *S*-palmitoylation by ZDHHCs can be stochastic, proximity based and lacking in
489 stereo-selectivity (Rocks et al., 2010; Rodenburg et al., 2017). Contrasting studies have shown that
490 numerous ZDHHCs have specific protein interacting domains including ankyrin repeat (AR), PDZ and SH3
491 domains that facilitate substrate interactions, providing support for a model in which more specific
492 enzyme-substrate interactions can govern *S*-palmitoylation (Abrami et al., 2017; Lemonidis et al., 2015;
493 Plain et al., 2020; Rana et al., 2018; Thomas et al., 2012; Verardi et al., 2017). Furthermore, a recent study

494 found striking substrate specificity for several ZDHHCs with the G-protein subunit Gαo, and revealed
495 intriguing observations that the subcellular localization of a number of *S*-palmitoylation substrates could
496 be controlled by changing the localization, and importantly, the expression of certain ZDHHC enzymes. In
497 this study, *S*-palmitoylated substrates were found to accumulate in the subcellular compartment in which
498 their partner ZDHHCs were targeted (Solis et al., 2020). This is particularly relevant as the ZDHHCs are
499 known to have diverse subcellular localizations including the Golgi, ER, endosomes and plasma membrane
500 (Globa and Bamji, 2017). Transcriptional control of differentially compartmentalized palmitoylating and
501 de-palmitoylating enzymes could therefore be an essential mechanism for regulating the subcellular
502 localization, and function, of *S*-palmitoylated protein substrates. Accordingly, LOF mutations in certain
503 ZDHHC enzymes leads to cell type-specific disruption in *S*-palmitoylation that is not compensated by other
504 members of the large ZDHHC family. We provide a means to investigate the expression of the proteins
505 that mediate *S*-palmitoylation, making BrainPalmSeq an invaluable resource to both researchers and
506 clinicians that are working to better understand the role of *S*-palmitoylation in the brain.

507

508 **Figure Legends**

509 **Figure 1. Heterogeneous ZDHHC expression in the mouse nervous system**

510 (A) Heatmap showing expression for the 24 ZDHHC genes, extracted from scRNAseq study of mouse CNS
511 and PNS (Zeisel et al., 2018). Each column represents one of the 265 metacells classified in the study.
512 Metacells are organized along x-axis according to hierarchical clustering designations generated by Zeisel
513 et al. Full metadata for this study available on BrainPalmSeq.

514 (B) Heatmap showing mean ZDHHC expression per hierarchical cluster, with columns and rows sorted by
515 descending mean ZDHHC expression per row/column.

516 (C) Heatmap showing mean ZDHHC expression per neurotransmitter cluster for all PNS and CNS neurons.
517 Columns and rows are sorted as in B.

518 (D) Correlation network showing ZDHHC co-expression across all metacells in 'MouseBrain' (Spearman R
519 > 0.5). Numbers in nodes correspond to ZDHHC number. Node color represents mean expression across
520 all metacells. Edge thickness represents strength of correlation.

521 (E) Graph showing proportion of genes from 'MouseBrain' dataset that are co-expressed with one or more
522 ZDHHC and also substrates for *S*-palmitoylation (SwissPalm annotated). 'Brain expressed' *n* = 15,389
523 protein coding genes expressed in the postnatal mouse brain, curated from the MGI RNAseq studies
524 database. 'R > 0.7 ZDHHC co-expressed' *n* = 914 genes co-expressed with one or more ZDHHC (Spearman
525 R > 0.7). 'R > 0.8 ZDHHC co-expressed' *n* = 167 genes co-expressed with one or more ZDHHC (Spearman R
526 > 0.8). Brain expressed vs. R > 0.7: $p < 0.001$; R > 0.7 vs R > 0.8: $p < 0.01$; Fisher's exact test.

527 (F) Graph of GO biological process analysis. Gene IDs from the 'MouseBrain' dataset (Zeisel et al., 2018)
528 that showed correlated expression with one or more ZDHHC (R > 0.7) and were also Uniprot reviewed and
529 SwissPalm annotated were used as input.

530 Units for all heatmaps in figure: mean log2(counts per 10,000 + 1).

531 **Figure 2. Diversity in ZDHHC expression and S-palmitoylation substrate expression in the hippocampus**

532 (A) Heatmap of excitatory neuron ZDHHC expression from dorsal hippocampus (original pooled cell
533 RNAseq data from Cembrowski et al., 2016) projected onto diagrams of dorsal hippocampus.

534 (B) Hierarchical clustering of ZDHHC expression data in A.

535 (C) Heatmap showing top 6 ranked expressing ZDHHCs in dorsal CA1 in descending order.

536 (D) Pie chart showing proportion genes with enriched expression in dorsal CA1 (dCA1) that are also
537 substrates for palmitoylation (SwissPalm annotated).

538 (E) KEGG analysis of the dCA1 enriched/SwissPalm annotated genes.

539 (F) SynGO analysis of the dCA1 enriched/SwissPalm annotated genes.

540 (G-J) As in (C)-(F) but for the dorsal dentate gyrus (dDG).

541 Heatmap legend in (A) applies to all heatmaps (logFKPM+1).

542 **Figure 3. Pyramidal neuron layer specific ZDHHC expression**

543 (A) Heatmap of excitatory neuron ZDHHC expression from somatosensory cortex (original data scRNAseq
544 data from Zeisel et al., 2015) projected onto diagrams of cortical layers.

545 (B) Hierarchical clustering of ZDHHC expression data in A. Heatmap units in (A, B): mean log2(counts per
546 10,000 + 1)

547 (C) Heatmap of scRNAseq data from Allen Brain 10X genomics (Yao et al., 2021). Data are represented as
548 mean ZDHHC expression per excitatory neuron subtype, with columns and rows sorted by descending
549 mean ZDHHC expression per row/column.

550 (D) As in (C) but for inhibitory neuron subtypes. Heatmap units for (C, D): trimmed mean (25%-75%)
551 Log2(CPM+1)

552 **Figure 4. Heterogeneous de-palmitoylating enzyme and ZDHHC accessory protein expression in the**
553 **mouse nervous system**

554 (A) Heatmap showing expression of de-palmitoylating enzymes (top) and ZDHHC accessory subunits
555 (bottom), extracted from scRNAseq study of mouse CNS and PNS (Zeisel et al., 2018). Each column
556 represents one of the 265 metacells classified in the study. Metacells are organized according to
557 hierarchical clustering designations generated by Zeisel et al.

558 (B) Heatmap showing mean de-palmitoylating enzyme expression per hierarchical cluster, with columns
559 and rows sorted by descending mean ZDHHC expression per row/column.

560 (C) As B but for ZDHHC accessory proteins.

561 (D) Correlation network showing ZDHHC co-expression with de-palmitoylating enyzmes and accessory
562 proteins across all metacells in 'MouseBrain' (Spearman R > 0.4). Node color represents mean expression
563 across all metacells. Edge thickness represents strength of correlation.

564 **Figure 5. Disease associated palmitoylating enzyme regional and cell-type expression overlays with**
565 **brain pathology in associated LOF disorders**

566 (A) Heatmap showing ranked *Zdhhc8* expressing neuronal and glial cell types in descending order. Original
567 data from scRNAseq neonatal mouse brain study; Rosenberg et al., 2018. Cell types were averaged as
568 described in Supplementary File 3. Heatmap units: mean log2(counts per 10,000 + 1).

569 (B) As in A, but original data from scRNAseq adolescent mouse brain study Zeisel et al (2018). Heatmap
570 units: mean log2(counts per 10,000 + 1).

571 (C) Heatmap of *Zdhhc8* expression from whole brain regional bulk RNAseq data (original data from
572 'Protein Atlas'; Sjöstedt et al., 2020) projected onto anatomical map of mouse brain. Heatmap units:
573 pTPM.

574 (D-F) As in (A)-(C) but for *Zdhhc9*.

575 (G-I) As in (A)-(C) but for *Ppt1*.

576 **Figure 6. Validation of predicted *S*-palmitoylation substrates of *Zdhhc9* derived from cell-type**
577 **enriched expression**

578 (A) Graph of expression data for *Zdhhc9* extracted from BrainPalmSeq. Original data from oligodendrocyte
579 scRNAseq study by Marques et al. Expression units: mean log2(counts per 10,000 + 1).

580 (B) Diagram illustrating workflow to generate a list of oligodendrocyte enriched palmitoylation
581 substrates, GO annotated for myelin sheath for experimental validation.

582 (C) STRING diagram of myelin sheath annotated palmitoylation substrates.

583 (D) Western blot following Acyl-RAC palmitoylation assay in HEK293 cells to identify palmitoylated and
584 unpalmitoylated fractions of FLAG-MOBP either without or with co-transfection of FLAG-GOLGA7 and
585 HA-ZDHHC9. Input = unprocessed protein lysate. NSB control = non-specific binding of unpalmitoylated
586 protein to sepharose resin in control pipeline. Palm fraction = palmitoylated protein (bound to
587 sepharose resin). Unpalm fraction = unpalmitoylated protein (did not bind to sepharose resin).

588 (E-F) As in (D) but for FLAG-PLP1 (E) or FLAG-CNP (F).

589 (G) Graphs quantifying the ratio of palmitoylated to unpalmitoylated protein either with or without co-
590 transfections with FLAG-GOLGA7 and HA-ZDHHC9. *n* = 4-6 HEK cell cultures per condition. Statistics
591 shown for palmitoylated fraction. Two-way ANOVA; Šídák's *post hoc*; mean ± SEM. MOBP: p = 0.0004,
592 95% CI -0.6594 to -0.2266; PLP1: p = 0.0046, 95% CI -0.1660 to -0.03011; CNP: p = 0.6981, 95% CI -
593 0.3274 to 0.1742.

594 **Source Data Legends**

595 **Figure 1 – Source data 1.** ZDHHC expression in the mouse nervous system

596 **Figure 2 – Source data 1.** ZDHHC expression and S-palmitoylation substrate expression in the
597 hippocampus

598 **Figure 3 – Source data 1.** ZDHHC expression cortical neurons

599 **Figure 4 – Source data 1.** De-palmitoylating enzyme and ZDHHC accessory protein expression in the
600 mouse nervous system

601 **Figure 5 – Source data 1.** Disease associated palmitoylating enzyme regional and cell-type expression
602 patterns

603 **Figure 6 – Source data 1.** Validation of predicted *S*-palmitoylation substrates of *Zdhhc9*

Materials and Methods

Data processing for BrainPalmSeq

For Zeisel et al., 2018 ('MouseBrain'), single-cell counts (UMI from 3' end counting) were downloaded from MouseBrain.org (loom file named l5_all.loom), and log normalized by first scaling the expression values provided to a sum of 10,000 per cell before calculating log2(scaled_counts+1). Averages were then performed by brain region, neurotransmitter and taxonomy for each gene.

For DropVIz Metacell counts were downloaded from DropViz.org (count file metacells.BrainCellAtlas_Saunders_version_2018.04.01.RDS and annotation file annotation.BrainCellAtlas_Saunders_version_2018.04.01.RDS) and log normalized by first scaling the expression values provided to a sum of 10,000 per metacell before calculating log2(scaled_counts+1). Averages were then performed by cell type, tissue and class for each gene. Genes associated with palmitoylation were selected in order to create the heatmaps.

For Zeisel, single-cell counts (UMI from 3' end counting) were downloaded from https://storage.googleapis.com/linnarsson-lab-www-blobs/blobs/cortex/expression_mRNA_17-Aug-2014.txt, and log normalized by first scaling the expression values provided to a sum of 10,000 per cell before calculating log2(scaled_counts+1). Averages were then performed by cluster, tissue and class for each gene. Genes associated with palmitoylation were selected in order to create the heatmaps, categories comprising fewer than 5 single cells are not displayed.

For Marques, single-cell counts (UMI from 3' end counting) were downloaded from GEO with accession ID GSE75330 (file GSE75330_Marques_et_al_mol_counts2.tab) and log normalized by first scaling the expression values provided to a sum of 10,000 per cell before calculating log2(scaled_counts+1). Averages were then performed by cluster and region for each gene. Genes associated with palmitoylation were selected in order to create the heatmaps, categories comprising fewer than 5 single cells are not displayed.

For Rosenberg, single-cell counts (UMI from 3' end counting) were downloaded from GSE110823, and log normalized by first scaling the expression values provided to a sum of 10,000 per cell before calculating log2(scaled_counts+1). Averages were then performed by brain region, neurotransmitter and taxonomy for each gene. Genes associated with palmitoylation were selected in order to create the heatmaps.

Data from Sjöstedt el al. were downloaded as Protein-coding transcripts per million (pTPM) from proteinatlas.org ("RNA mouse brain region gene data") and not further processed.

For Hipposeq, expression data were downloaded as FKPM directly from hipposeq.janelia.org and were not further processed.

For Allen Brain 10X data, expression data were downloaded as trimmed means (25%-75%) Log2(CPM+1) from portal.brain-map.org/ and were not further processed.

Correlation analysis

Spearman correlation values between genes and their significances were calculated in R using the expression results obtained for each cell type as described above.

640 **Identification of *S*-palmitoylation substrates with SwissPalm**

641 Gene lists were inputted into SwissPalm (https://swisspalm.org/proteins) input file function and cross-
642 referenced with 'Dataset 3: Palmitoylation validated or found in at least one palmitoyl-proteome
643 (SwissPalm annotated)' for *Mus musculus*, with an additional filter for UniProt 'Reviewed' proteins.

644 **Generating a predicted palmitoylome for dorsal hippocampus**

645 To curate the regionally enriched predicted-palmitoylome, the enrichment analysis tools in hipposeq
646 (https://hipposeq.janelia.org/) were used to compare each of the selected Cell Lines vs the other Cell Lines
647 in the analysis (Selected Cell Lines = dorsal DG, CA3, CA2 and CA1), with the following parameters: 'Fold
648 threshold' = 1.5; 'FKPMmin threshold' = 5, 'FDR' = 0.05. The resulting lists of regionally enriched transcripts
649 were cross referenced with SwissPalm as described above to identify regionally enriched *S*-palmitoylation
650 substrates.

651 **Bioinformatic analysis**

652 Gene Ontology (GO) analysis was performed using statistical overrepresentation tests in PANTHER16.0
653 (Mi et al., 2009) with default settings and *Mus musculus* as the reference species. Biological process GO
654 terms were extracted and ranked according to false discovery rate (FDR). Kyoto Encyclopedia of Genes
655 and Genomes (KEGG) analysis was performed using the web-based program Enrichr (Chen et al., 2013;
656 Kuleshov et al., 2016) and ranked according to -log Adjusted P-value. Synaptic Gene Ontologies (SynGO;
657 version 1.1) analysis was performed using default settings with brain expressed genes as a background
658 and terms for 'biological process' were ranked according to -log Adjusted P-value. Functional protein
659 interaction networks were identified using the Search Tool for the Retrieval of Interacting Genes (STRING)
660 11.0 (Szklarczyk et al., 2019) with *Mus musculus* as the reference species. Seven types of protein
661 interactions were used for network generation, including text mining, neighborhood, co-occurrence, co-
662 expression, gene fusion, experiments and databases.

663 **Data presentation**

664 Heatmaps were plotted and hierarchical clustering performed in Displayr (https://www.displayr.com)
665 using the 'Dendrogram' function. Cytoscape (Version 3.8.0) was used to draw correlation networks.

666 **Heatmap creation for BrainPalmSeq**

667 All plots for the BrainPalmSeq database were generated using curated RNA sequencing datasets. Python
668 3 and Javascript scripts were used with the plotting library Bokeh to generate the interactive heatmaps to
669 display and compare these datasets on the BrainPalmSeq website (Bokeh Development Team, 2018).

670 **Cell culture**

671 HEK293T cells were thawed and aliquoted into a 10cm dish with 10mL prewarmed (37°C) DMEM
672 (GIBCO, Thermo Fisher Scientific, Waltham, MA) supplemented with 10% fetal bovine serum (FBS)
673 (GIBCO, Thermo Fisher Scientific, Waltham, MA) and 1% Pen/Strep(P/S) (GIBCO, Thermo Fisher
674 Scientific, Waltham, MA). HEK293T cells were then placed in a 37°C incubator with 5% CO2 and
675 passaged approximately every 5 days, or once confluency was achieved.

676 **Transfection**

677 70%-80% confluent HEK293T cells were transfected using Lipofectamine 2000 (Invitrogen/Life
678 Technologies, Carlsbad, CA) according to the manufacturer's recommendations. Each well of a 6-well
679 plate was transfected with a total of 3ug DNA, 150uL of Opti-Mem (GIBCO, Thermo Fisher Scientific,
680 Waltham, MA) was used with 6uL of Lipofectamine 2000 (Invitrogen/Life Technologies, Carlsbad, CA).
681 Experimental condition wells were transfected with 1ug of the indicated construct of interest, 1ug of
682 HA-DHHC9 (mouse; Shimell et al., 2019), and 1ug of FLAG-GOLGA7 (Maurine Linder, Washington
683 University School of Medicine). Human FLAG-MOBP (CAT#: RC223946), FLAG-PLP1 (CAT#: RC218616)
684 and FLAG-CNP (CAT#: RC207038) were acquired from Origene, Maryland, USA. Control condition wells
685 were transfected with 1ug of the indicated construct of interest, and 2ug of a scrambled control
686 plasmid. Cells were lysed using the acyl-RAC assay lysis buffer 48hours after transfection.

687 **Palmitoylation Assay (acyl-RAC)**

688 The commercially available CAPTUREome S-palmitoylated protein kit (Badrilla, Leeds, UK) was used in
689 accordance with the manufacturer's guidelines with three optimizations: (1) prior to the cell lysis step,
690 wells were washed with 1mL of 1X PBS to eliminate any dead cells or residual media; (2) during the cell
691 lysis step, DNase (Sigma-Aldrich, St. Louis, MO), was added to the solution (5uL per 500uL of lysis
692 buffer); and (2) protein concentration was measured prior to the separation of experimental sample and
693 negative control sample using the BCA Assay (Pierce, Thermo Fisher Scientific, Waltham, MA).

694 **Western Blot Analysis**

695 Western blotting was performed using 4% stacking and 12% resolving SDS-PAGE gels. PVDF membranes
696 were then blocked for 1hour at room temperature with 5% BSA in 0.05% TBS-T. PVDF membranes were
697 incubated with the indicated primary antibodies (anti-HA: Cell Signaling Technology, C29F4, Rabbit mAb
698 CAT#: 3724, 1:1000; anti-FLAG: Origene, mouse monoclonal antibody, CAT#: TA50011-100, 1:1000)
699 overnight at 4°C. Proteins were then visualized using enhanced chemiluminescence (Immubilon Western
700 Chemiluminescent HRP Substrate) on a BioRad ChemiDoc XRS+ scanner. Blots were then quantified
701 using Fiji1 software. The palmitoylated and unpalmitoylated fractions were calculated using the
702 following equations respectively: (Palm Fraction / (Palm Fraction + Unpalm Fraction)) and (Unpalm
703 Fraction / (Palm Fraction + Unpalm Fraction)). Criteria for data inclusion were sufficient
704 transfection/antibody signal and minimal protein in the non-specific binding control.

705 **Statistical Analysis**

706 Spearman correlations were performed with the function cor in R, and their significances were obtained
707 using the function cor.test followed by a correction for multiple testing using p.adjust with the fdr
708 method (Benjamini & Hochberg). For assessing enrichment of *S*-palmitoylation substrates within Zdhhc
709 co-expressed genes, Fisher's exact test was performed using the function fisher.test in R.

710 For validation of substrates using Acyl-Rac palmitoylation assay, two-way ANOVA with Šídák's *post hoc*
711 was used to assess significance of both palmitoylated and unpalmitoylated fractions. Statistics are
712 shown for palmitoylated fraction. No outliers were excluded. Statistical analyses were performed in
713 GraphPad Prism 9.2.0 (San Diego, CA, USA). *n* represents the number of individual HEK cell culture
714 dishes. Each culture dish is defined as a biological replicate. No technical replicates were performed.

Acknowledgements

The authors would like to thank Drs. A. Ciernia, M. Cembrowski, T. Murphy and J. LeDue for helpful discussion. This work was supported by CIHR Foundation grant (F18-00650) to SXB and by computational resources made available through the NeuroImaging and NeuroComputation Centre at the Djavad Mowafaghian Centre for Brain Health (RRID SCR_019086) and the Dynamic Brain Circuits in Health and Disease Research Excellence Cluster DataBinge Forum.

721 **References**

722 Abrami L, Dallavilla T, Sandoz PA, Demir M, Kunz B, Savoglidis G, Hatzimanikatis V, van Der Goot FG.
723 2017. Identification and dynamics of the human ZDHHC16-ZDHHC6 palmitoylation cascade. *eLife* **6**.
724 doi:10.7554/eLife.27826

725 Baker K, Astle DE, Scerif G, Barnes J, Smith J, Moffat G, Gillard J, Baldeweg T, Raymond FL. 2015.
726 Epilepsy, cognitive deficits and neuroanatomy in males with ZDHHC9 mutations. *Annals of Clinical*
727 *and Translational Neurology* **2**:559–569. doi:10.1002/acn3.196

728 Bathelt J, Astle D, Barnes J, Raymond FL, Baker K. 2016. Structural brain abnormalities in a single gene
729 disorder associated with epilepsy, language impairment and intellectual disability. *NeuroImage:*
730 *Clinical* **12**:655–665. doi:10.1016/j.nicl.2016.07.016

731 Bathelt J, Barnes J, Raymond FL, Baker K, Astle D. 2017. Global and Local Connectivity Differences
732 Converge With Gene Expression in a Neurodevelopmental Disorder of Known Genetic Origin.
733 *Cerebral Cortex* **27**:3806–3817. doi:10.1093/cercor/bhx027

734 Bird CM, Burgess N. 2008. The hippocampus and memory: Insights from spatial processing. *Nature*
735 *Reviews Neuroscience* **9**:182–194. doi:10.1038/nrn2335

736 Blanc M, David F, Abrami L, Migliozzi D, Armand F, Bürgi J, van der Goot FG. 2015. SwissPalm: Protein
737 Palmitoylation database. *F1000Research* **4**. doi:10.12688/f1000research.6464.1

738 Blanc M, David FPA, van der Goot FG. 2019. SwissPalm 2: Protein S-palmitoylation databaseMethods in
739 Molecular Biology. Humana Press Inc. pp. 203–214. doi:10.1007/978-1-4939-9532-5_16

740 Chen EY, Tan CM, Kou Y, Duan Q, Wang Z, Meirelles G V., Clark NR, Ma'ayan A. 2013. Enrichr: Interactive
741 and collaborative HTML5 gene list enrichment analysis tool. *BMC Bioinformatics* **14**.
742 doi:10.1186/1471-2105-14-128

743 Chen WY, Shi YY, Zheng YL, Zhao XZ, Zhang GJ, Chen SQ, Yang P Di, He L. 2004. Case-control study and
744 transmission disequilibrium test provide consistent evidence for association between
745 schizophrenia and genetic variation in the 22q11 gene ZDHHC8. *Human Molecular Genetics*
746 **13**:2991–2995. doi:10.1093/hmg/ddh322

747 Cho E, Park M. 2016. Palmitoylation in Alzheimer's disease and other neurodegenerative diseases.
748 *Pharmacological Research* **111**:133–151. doi:10.1016/j.phrs.2016.06.008

749 Forrester MT, Hess DT, Thompson JW, Hultman R, Moseley MA, Stamler JS, Casey PJ. 2011. Site-specific
750 analysis of protein S-acylation by resin-assisted capture. *Journal of Lipid Research* **52**:393–398.
751 doi:10.1194/JLR.D011106/ATTACHMENT/AA2B322B-A63D-41C0-A864-92DAC7C09076/MMC1.PDF

752 Fredericks G, Hoffmann F, Hondal R, Rozovsky S, Urschitz J, Hoffmann P. 2017. Selenoprotein K Increases
753 Efficiency of DHHC6 Catalyzed Protein Palmitoylation by Stabilizing the Acyl-DHHC6 Intermediate.
754 *Antioxidants* **7**:4. doi:10.3390/antiox7010004

755 Fredericks GJ, Hoffmann FKW, Rose AH, Osterheld HJ, Hess FM, Mercier F, Hoffmann PR. 2014. Stable
756 expression and function of the inositol 1,4,5-triphosphate receptor requires palmitoylation by a
757 DHHC6/selenoprotein K complex. *Proceedings of the National Academy of Sciences of the United*
758 *States of America* **111**:16478–16483. doi:10.1073/pnas.1417176111

759 Fukata Y, Dimitrov A, Boncompain G, Vielemeyer O, Perez F, Fukata M. 2013. Local palmitoylation cycles
760 define activity-regulated postsynaptic subdomains. *Journal of Cell Biology* **202**:145–161.
761 doi:10.1083/jcb.201302071

762 Fukata Y, Fukata M. 2010. Protein palmitoylation in neuronal development and synaptic plasticity.
763 *Nature Reviews Neuroscience* **11**:161–175. doi:10.1038/nrn2788

764 Glantz LA, Lewis DA. 2000. Decreased dendritic spine density on prefrontal cortical pyramidal neurons in
765 schizophrenia. *Archives of General Psychiatry* **57**:65–73. doi:10.1001/archpsyc.57.1.65

766 Globa AK, Bamji SX. 2017. Protein palmitoylation in the development and plasticity of neuronal
767 connections. *Current Opinion in Neurobiology* **45**:210–220. doi:10.1016/j.conb.2017.02.016

768 Gorinski N, Bijata M, Prasad S, Wirth A, Abdel Galil D, Zeug A, Bazovkina D, Kondaurova E, Kulikova E,
769 Ilchibaeva T, Zareba-Koziol M, Papaleo F, Scheggia D, Kochlamazashvili G, Dityatev A, Smyth I,
770 Krzystyniak A, Wlodarczyk J, Richter DW, Strekalova T, Sigrist S, Bang C, Hobuß L, Fiedler J, Thum T,
771 Naumenko VS, Pandey G, Ponimaskin E. 2019. Attenuated palmitoylation of serotonin receptor 5-
772 HT1A affects receptor function and contributes to depression-like behaviors. *Nature*
773 *Communications* **10**:1–14. doi:10.1038/s41467-019-11876-5

774 Haque A, Engel J, Teichmann SA, Lönnberg T. 2017. A practical guide to single-cell RNA-sequencing for
775 biomedical research and clinical applications. *Genome Medicine* **9**:1–12. doi:10.1186/s13073-017-
776 0467-4

Harris KD, Shepherd GMG. 2015. The neocortical circuit: Themes and variations. *Nature Neuroscience* **18**:170–181. doi:10.1038/nn.3917

Ji B, Skup M. 2021. Roles of palmitoylation in structural long-term synaptic plasticity. *Molecular Brain* **14**:1–27. doi:10.1186/s13041-020-00717-y

Kang R, Wan J, Arstikaitis P, Takahashi H, Huang K, Bailey AO, Thompson JX, Roth AF, Drisdel RC, Mastro R, Green WN, Yates JR, Davis NG, El-Husseini A. 2008. Neural palmitoyl-proteomics reveals dynamic synaptic palmitoylation. *Nature* **456**:904–909. doi:10.1038/nature07605

Karayiorgou M, Simon TJ, Gogos JA. 2010. 22q11.2 microdeletions: Linking DNA structural variation to brain dysfunction and schizophrenia. *Nature Reviews Neuroscience* **11**:402–416. doi:10.1038/nrn2841

Kolluri N, Sun Z, Sampson AR, Lewis DA. 2005. Lamina-specific reductions in dendritic spine density in the prefrontal cortex of subjects with schizophrenia. *American Journal of Psychiatry* **162**:1200–1202. doi:10.1176/appi.ajp.162.6.1200

Koopmans F, van Nierop P, Andres-Alonso M, Byrnes A, Cijsouw T, Coba MP, Cornelisse LN, Farrell RJ, Goldschmidt HL, Howrigan DP, Hussain NK, Imig C, de Jong APH, Jung H, Kohansalnodehi M, Kramarz B, Lipstein N, Lovering RC, MacGillavry H, Mariano V, Mi H, Ninov M, Osumi-Sutherland D, Pielot R, Smalla KH, Tang H, Tashman K, Toonen RFG, Verpelli C, Reig-Viader R, Watanabe K, van Weering J, Achsel T, Ashrafi G, Asi N, Brown TC, De Camilli P, Feuermann M, Foulger RE, Gaudet P, Joglekar A, Kanellopoulos A, Malenka R, Nicoll RA, Pulido C, de Juan-Sanz J, Sheng M, Südhof TC, Tilgner HU, Bagni C, Bayés À, Biederer T, Brose N, Chua JJE, Dieterich DC, Gundelfinger ED, Hoogenraad C, Huganir RL, Jahn R, Kaeser PS, Kim E, Kreutz MR, McPherson PS, Neale BM, O'Connor V, Posthuma D, Ryan TA, Sala C, Feng G, Hyman SE, Thomas PD, Smit AB, Verhage M. 2019. SynGO: An Evidence-Based, Expert-Curated Knowledge Base for the Synapse. *Neuron* **103**:217-234.e4. doi:10.1016/j.neuron.2019.05.002

Koster KP, Yoshii A. 2019. Depalmitoylation by palmitoyl-protein thioesterase 1 in neuronal health and degeneration. *Frontiers in Synaptic Neuroscience* **11**:25. doi:10.3389/fnsyn.2019.00025

Kouskou M, Thomson DM, Brett RR, Wheeler L, Tate RJ, Pratt JA, Chamberlain LH. 2018. Disruption of the Zdhhc9 intellectual disability gene leads to behavioural abnormalities in a mouse model. *Experimental Neurology* **308**:35–46. doi:10.1016/J.EXPNEUROL.2018.06.014

806 Kuleshov M V., Jones MR, Rouillard AD, Fernandez NF, Duan Q, Wang Z, Koplev S, Jenkins SL, Jagodnik
807 KM, Lachmann A, McDermott MG, Monteiro CD, Gundersen GW, Ma'ayan A. 2016. Enrichr: a
808 comprehensive gene set enrichment analysis web server 2016 update. *Nucleic acids research*
809 **44**:W90–W97. doi:10.1093/nar/gkw377

810 Lemonidis K, Sanchez-Perez MC, Chamberlain LH. 2015. Identification of a novel sequence motif
811 recognized by the ankyrin repeat domain of zDHHC17/13 S-acyltransferases. *Journal of Biological*
812 *Chemistry* **290**:21939–21950. doi:10.1074/jbc.M115.657668

813 Lin DTS, Conibear E. 2015. ABHD17 proteins are novel protein depalmitoylases that regulate N-Ras
814 palmitate turnover and subcellular localization. *eLife* **4**. doi:10.7554/eLife.11306

815 Lu JY, Verkruyse LA, Hofmann SL. 1996. Lipid thioesters derived from acylated proteins accumulate in
816 infantile neuronal ceroid lipofuscinosis: Correction of the defect in lymphoblasts by recombinant
817 palmitoyl-protein thioesterase. *Proceedings of the National Academy of Sciences of the United*
818 *States of America* **93**:10046–10050. doi:10.1073/pnas.93.19.10046

819 Ma Y, Liu H, Ou Z, Qi C, Xing R, Wang S, Han Y, Zhao T-J, Chen Y. 2021. DHHC5 facilitates oligodendrocyte
820 development by palmitoylating and activating STAT3. *Glia*. doi:10.1002/glia.24113

821 Malgapo MIP, Linder ME. 2021. Substrate recruitment by zDHHC protein acyltransferases. *Open Biology*
822 **11**:rsob.210026. doi:10.1098/rsob.210026

823 Marques S, Zeisel A, Codeluppi S, Van Bruggen D, Falcão AM, Xiao L, Li H, Häring M, Hochgerner H,
824 Romanov RA, Gyllborg D, Muñoz-Manchado AB, La Manno G, Lönnerberg P, Floriddia EM, Rezayee
825 F, Ernfors P, Arenas E, Hjerling-Leffler J, Harkany T, Richardson WD, Linnarsson S, Castelo-Branco G.
826 2016. Oligodendrocyte heterogeneity in the mouse juvenile and adult central nervous system.
827 *Science* **352**:1326–1329. doi:10.1126/science.aaf6463

828 Matt L, Kim K, Chowdhury D, Hell JW. 2019. Role of palmitoylation of postsynaptic proteins in promoting
829 synaptic plasticity. *Frontiers in Molecular Neuroscience*. doi:10.3389/fnmol.2019.00008

830 Mi H, Dong Q, Muruganujan A, Gaudet P, Lewis S, Thomas PD. 2009. PANTHER version 7: Improved
831 phylogenetic trees, orthologs and collaboration with the Gene Ontology Consortium. *Nucleic Acids*
832 *Research* **38**. doi:10.1093/nar/gkp1019

833 Mitchell DA, Hamel LD, Reddy KD, Farh L, Rettew LM, Sanchez PR, Deschenes RJ. 2014. Mutations in the

X-linked intellectual disability gene, zDHHC9, alter autopalmitoylation activity by distinct mechanisms. *Journal of Biological Chemistry* **289**:18582–18592. doi:10.1074/jbc.M114.567420

Mukai J, Liu H, Burt RA, Swor DE, Lai WS, Karayiorgou M, Gogos JA. 2004. Evidence that the gene encoding ZDHHC8 contributes to the risk of schizophrenia. *Nature Genetics* **36**:725–731. doi:10.1038/ng1375

Nita DA, Mole SE, Minassian BA. 2016. Neuronal ceroid lipofuscinoses. *Epileptic Disorders* **18**:S73–S88. doi:10.1684/epd.2016.0844

Pitts MW, Hoffmann PR. 2018. Endoplasmic reticulum-resident selenoproteins as regulators of calcium signaling and homeostasis. *Cell Calcium* **70**:76–86. doi:10.1016/j.ceca.2017.05.001

Plain F, Howie J, Kennedy J, Brown E, Shattock MJ, Fraser NJ, Fuller W. 2020. Control of protein palmitoylation by regulating substrate recruitment to a zDHHC-protein acyltransferase. *Communications Biology* **3**:1–10. doi:10.1038/s42003-020-01145-3

Rana MS, Lee CJ, Banerjee A. 2018. The molecular mechanism of DHHC protein acyltransferases. *Biochemical Society Transactions* **47**:157–167. doi:10.1042/BST20180429

Raymond FL, Tarpey PS, Edkins S, Tofts C, O'Meara S, Teague J, Butler A, Stevens C, Barthorpe S, Buck G, Cole J, Dicks E, Gray K, Halliday K, Hills K, Hinton J, Jones D, Menzies A, Perry J, Raine K, Shepherd R, Small A, Varian J, Widaa S, Mallya U, Moon J, Luo Y, Shaw M, Boyle J, Kerr B, Turner G, Quarrell O, Cole T, Easton DF, Wooster R, Bobrow M, Schwartz CE, Gecz J, Stratton MR, Futreal PA. 2007. Mutations in ZDHHC9, Which Encodes a Palmitoyltransferase of NRAS and HRAS, Cause X-Linked Mental Retardation Associated with a Marfanoid Habitus. *The American Journal of Human Genetics* **80**:982–987. doi:10.1086/513609

Roberts MS, Macauley SL, Wong AM, Yilmas D, Hohm S, Cooper JD, Sands MS. 2012. Combination small molecule PPT1 mimetic and CNS-directed gene therapy as a treatment for infantile neuronal ceroid lipofuscinosis. *Journal of Inherited Metabolic Disease* **35**:847–857. doi:10.1007/s10545-011-9446-x

Rocks O, Gerauer M, Vartak N, Koch S, Huang ZP, Pechlivanis M, Kuhlmann J, Brunsveld L, Chandra A, Ellinger B, Waldmann H, Bastiaens PIH. 2010. The palmitoylation machinery is a spatially organizing system for peripheral membrane proteins. *Cell* **141**:458–471. doi:10.1016/j.cell.2010.04.007

Rodenburg RNP, Snijder J, Van De Waterbeemd M, Schouten A, Granneman J, Heck AJR, Gros P. 2017.

862 Stochastic palmitoylation of accessible cysteines in membrane proteins revealed by native mass
863 spectrometry. *Nature Communications* **8**:1–9. doi:10.1038/s41467-017-01461-z

864 Rosenberg AB, Roco CM, Muscat RA, Kuchina A, Sample P, Yao Z, Graybuck LT, Peeler DJ, Mukherjee S,
865 Chen W, Pun SH, Sellers DL, Tasic B, Seelig G. 2018. Single-cell profiling of the developing mouse
866 brain and spinal cord with split-pool barcoding. *Science* **360**:176–182.
867 doi:10.1126/science.aam8999

868 Salaun C, Locatelli C, Zmuda F, González JC, Chamberlain LH. 2020. Accessory proteins of the zDHHC
869 family of S-acylation enzymes. *Journal of Cell Science* **133**. doi:10.1242/jcs.251819

870 Sanders SS, Martin DDO, Butland SL, Lavallée-Adam M, Calzolari D, Kay C, Yates JR, Hayden MR. 2015.
871 Curation of the Mammalian Palmitoylome Indicates a Pivotal Role for Palmitoylation in Diseases
872 and Disorders of the Nervous System and Cancers. *PLoS Computational Biology* **11**:e1004405.
873 doi:10.1371/journal.pcbi.1004405

874 Saunders A, Macosko EZ, Wysoker A, Goldman M, Krienen FM, de Rivera H, Bien E, Baum M, Bortolin L,
875 Wang S, Goeva A, Nemesh J, Kamitaki N, Brumbaugh S, Kulp D, McCarroll SA. 2018. Molecular
876 Diversity and Specializations among the Cells of the Adult Mouse Brain. *Cell* **174**:1015-1030.e16.
877 doi:10.1016/j.cell.2018.07.028

878 Schneider A, Länder H, Schulz G, Wolburg H, Nave K-A, Schulz JB, Simons M. 2005. Palmitoylation is a
879 sorting determinant for transport to the myelin membrane. *Journal of cell science* **118**:2415–23.
880 doi:10.1242/jcs.02365

881 Schwarz F, Aebi M. 2011. Mechanisms and principles of N-linked protein glycosylation. *Current Opinion*
882 *in Structural Biology* **21**:576–582. doi:10.1016/j.sbi.2011.08.005

883 Shimell JJ, Shah BS, Cain SM, Thouta S, Kuhlmann N, Tatarnikov I, Jovellar DB, Brigidi GS, Kass J,
884 Milnerwood AJ, Snutch TP, Bamji SX. 2019. The X-Linked Intellectual Disability Gene Zdhhc9 Is
885 Essential for Dendrite Outgrowth and Inhibitory Synapse Formation. *Cell Reports* **29**:2422-2437.e8.
886 doi:10.1016/j.celrep.2019.10.065

887 Shyng C, Nelvagal HR, Dearborn JT, Tyynelä J, Schmidt RE, Sands MS, Cooper JD. 2017. Synergistic effects
888 of treating the spinal cord and brain in CLN1 disease. *Proceedings of the National Academy of*
889 *Sciences of the United States of America* **114**:E5920–E5929. doi:10.1073/pnas.1701832114

890 Sjöstedt E, Zhong W, Fagerberg L, Karlsson M, Mitsios N, Adori C, Oksvold P, Edfors F, Limiszewska A,
891 Hikmet F, Huang J, Du Y, Lin L, Dong Z, Yang L, Liu X, Jiang H, Xu X, Wang J, Yang H, Bolund L,
892 Mardinoglu A, Zhang C, von Feilitzen K, Lindskog C, Pontén F, Luo Y, Hökfelt T, Uhlén M, Mulder J.
893 2020. An atlas of the protein-coding genes in the human, pig, and mouse brain. *Science*
894 **367**:eaay5947. doi:10.1126/science.aay5947

895 Solis GP, Valnohova J, Alvarez C, Katanaev VL. 2020. Local and substrate-specific S-palmitoylation
896 determines subcellular localization of Gαo. *bioRxiv* 2020.08.25.266692.
897 doi:10.1101/2020.08.25.266692

898 Swarthout JT, Lobo S, Farh L, Croke MR, Greentree WK, Deschenes RJ, Linder ME. 2005. DHHC9 and
899 GCP16 constitute a human protein fatty acyltransferase with specificity for H- and N-Ras. *Journal of*
900 *Biological Chemistry* **280**:31141–31148. doi:10.1074/jbc.M504113200

901 Szklarczyk D, Gable AL, Lyon D, Junge A, Wyder S, Huerta-Cepas J, Simonovic M, Doncheva NT, Morris JH,
902 Bork P, Jensen LJ, Von Mering C. 2019. STRING v11: Protein-protein association networks with
903 increased coverage, supporting functional discovery in genome-wide experimental datasets.
904 *Nucleic Acids Research* **47**:D607–D613. doi:10.1093/nar/gky1131

905 Tasic B, Yao Z, Graybuck LT, Smith KA, Nguyen TN, Bertagnolli D, Goldy J, Garren E, Economo MN,
906 Viswanathan S, Penn O, Bakken T, Menon V, Miller J, Fong O, Hirokawa KE, Lathia K, Rimorin C,
907 Tieu M, Larsen R, Casper T, Barkan E, Kroll M, Parry S, Shapovalova N V., Hirschstein D, Pendergraft
908 J, Sullivan HA, Kim TK, Szafer A, Dee N, Groblewski P, Wickersham I, Cetin A, Harris JA, Levi BP,
909 Sunkin SM, Madisen L, Daigle TL, Looger L, Bernard A, Phillips J, Lein E, Hawrylycz M, Svoboda K,
910 Jones AR, Koch C, Zeng H. 2018. Shared and distinct transcriptomic cell types across neocortical
911 areas. *Nature* **563**:72–78. doi:10.1038/s41586-018-0654-5

912 Thomas GM, Hayashi T, Chiu SL, Chen CM, Huganir RL. 2012. Palmitoylation by DHHC5/8 Targets GRIP1
913 to Dendritic Endosomes to Regulate AMPA-R Trafficking. *Neuron* **73**:482–496.
914 doi:10.1016/j.neuron.2011.11.021

915 Thomas GM, Hayashi T, Huganir RL, Linden DJ. 2013. DHHC8-dependent PICK1 palmitoylation is required
916 for induction of cerebellar long-term synaptic depression. *Journal of Neuroscience* **33**:15401–
917 15407. doi:10.1523/JNEUROSCI.1283-13.2013

918 Tzschach A, Grasshoff U, Beck-Woedl S, Dufke C, Bauer C, Kehrer M, Evers C, Moog U, Oehl-Jaschkowitz

919 B, Donato N Di, Maiwald R, Jung C, Kuechler A, Schulz S, Meinecke P, Spranger S, Kohlhase J, Seidel
920 J, Reif S, Rieger M, Riess A, Sturm M, Bickmann J, Schroeder C, Dufke A, Riess O, Bauer P. 2015.
921 Next-generation sequencing in X-linked intellectual disability. *European Journal of Human Genetics*
922 **23**:1513–1518. doi:10.1038/ejhg.2015.5

923 Ubersax JA, Ferrell JE. 2007. Mechanisms of specificity in protein phosphorylation. *Nature Reviews*
924 *Molecular Cell Biology* **8**:530–541. doi:10.1038/nrm2203

925 Vartak N, Papke B, Grecco HE, Rossmannek L, Waldmann H, Hedberg C, Bastiaens PIH. 2014. The
926 autodepalmitoylating activity of APT maintains the spatial organization of palmitoylated
927 membrane proteins. *Biophysical Journal* **106**:93–105. doi:10.1016/j.bpj.2013.11.024

928 Verardi R, Kim JS, Ghirlando R, Banerjee A. 2017. Structural Basis for Substrate Recognition by the
929 Ankyrin Repeat Domain of Human DHHC17 Palmitoyltransferase. *Structure* **25**:1337-1347.e6.
930 doi:10.1016/j.str.2017.06.018

931 Virlogeux A, Scaramuzzino C, Lenoir S, Carpentier R, Louessard M, Genoux A, Lino P, Hinckelmann MV,
932 Perrier AL, Humbert S, Saudou F. 2021. Increasing brain palmitoylation rescues behavior and
933 neuropathology in Huntington disease mice. *Science Advances* **7**:799–830.
934 doi:10.1126/sciadv.abb0799

935 Wagstyl K, Ronan L, Whitaker KJ, Goodyer IM, Roberts N, Crow TJ, Fletcher PC. 2016. Multiple markers
936 of cortical morphology reveal evidence of supragranular thinning in schizophrenia. *Translational*
937 *Psychiatry* **6**:780. doi:10.1038/tp.2016.43

938 Woodley KT, Collins MO. 2019. S-acylated Golga7b stabilises <scp>DHHC</scp> 5 at the plasma
939 membrane to regulate cell adhesion. *EMBO reports* **20**:e47472. doi:10.15252/embr.201847472

940 Yanai A, Huang K, Kang R, Singaraja RR, Arstikaitis P, Gan L, Orban PC, Mullard A, Cowan CM, Raymond
941 LA, Drisdel RC, Green WN, Ravikumar B, Rubinsztein DC, El-Husseini A, Hayden MR. 2006.
942 Palmitoylation of huntingtin by HIP14is essential for its trafficking and function. *Nature*
943 *Neuroscience* **9**:824–831. doi:10.1038/nn1702

944 Yao Z, van Velthoven CTJ, Nguyen TN, Goldy J, Sedeno-Cortes AE, Baftizadeh F, Bertagnolli D, Casper T,
945 Chiang M, Crichton K, Ding SL, Fong O, Garren E, Glandon A, Gouwens NW, Gray J, Graybuck LT,
946 Hawrylycz MJ, Hirschstein D, Kroll M, Lathia K, Lee C, Levi B, McMillen D, Mok S, Pham T, Ren Q,
947 Rimorin C, Shapovalova N, Sulc J, Sunkin SM, Tieu M, Torkelson A, Tung H, Ward K, Dee N, Smith

948 KA, Tasic B, Zeng H. 2021. A taxonomy of transcriptomic cell types across the isocortex and
949 hippocampal formation. *Cell* **184**:3222-3241.e26. doi:10.1016/j.cell.2021.04.021

950 Yuan W, Lu L, Rao M, Huang Y, Liu CE, Liu S, Zhao Y, Liu H, Zhu J, Chao T, Wu C, Ren J, Lv L, Li W, Qi S,
951 Liang Y, Yue S, Gao J, Zhang Z, Kong E. 2021. GFAP hyperpalmitoylation exacerbates astrogliosis and
952 neurodegenerative pathology in PPT1-deficient mice. *Proceedings of the National Academy of*
953 *Sciences of the United States of America* **118**. doi:10.1073/pnas.2022261118

954 Zareba-Koziol M, Bartkowiak-Kaczmarek A, Figiel I, Krzystyniak A, Wojtowicz T, Bijata M, Wlodarczyk J.
955 2019. Stress-induced Changes in the S-palmitoylation and S-nitrosylation of Synaptic Proteins.
956 *Molecular and Cellular Proteomics* **18**:1916–1938. doi:10.1074/mcp.RA119.001581

957 Zeisel A, Hochgerner H, Lönnerberg P, Johnsson A, Memic F, van der Zwan J, Häring M, Braun E, Borm LE,
958 La Manno G, Codeluppi S, Furlan A, Lee K, Skene N, Harris KD, Hjerling-Leffler J, Arenas E, Ernfors P,
959 Marklund U, Linnarsson S. 2018. Molecular Architecture of the Mouse Nervous System. *Cell*
960 **174**:999-1014.e22. doi:10.1016/j.cell.2018.06.021

961 Zeisel A, M͡oz-Manchado AB, Codeluppi S, Lönnerberg P, Manno G La, Juréus A, Marques S, Munguba H,
962 He L, Betsholtz C, Rolny C, Castelo-Branco G, Hjerling-Leffler J, Linnarsson S. 2015. Cell types in the
963 mouse cortex and hippocampus revealed by single-cell RNA-seq. *Science* **347**:1138–1142.
964 doi:10.1126/science.aaa1934

965

Figure1

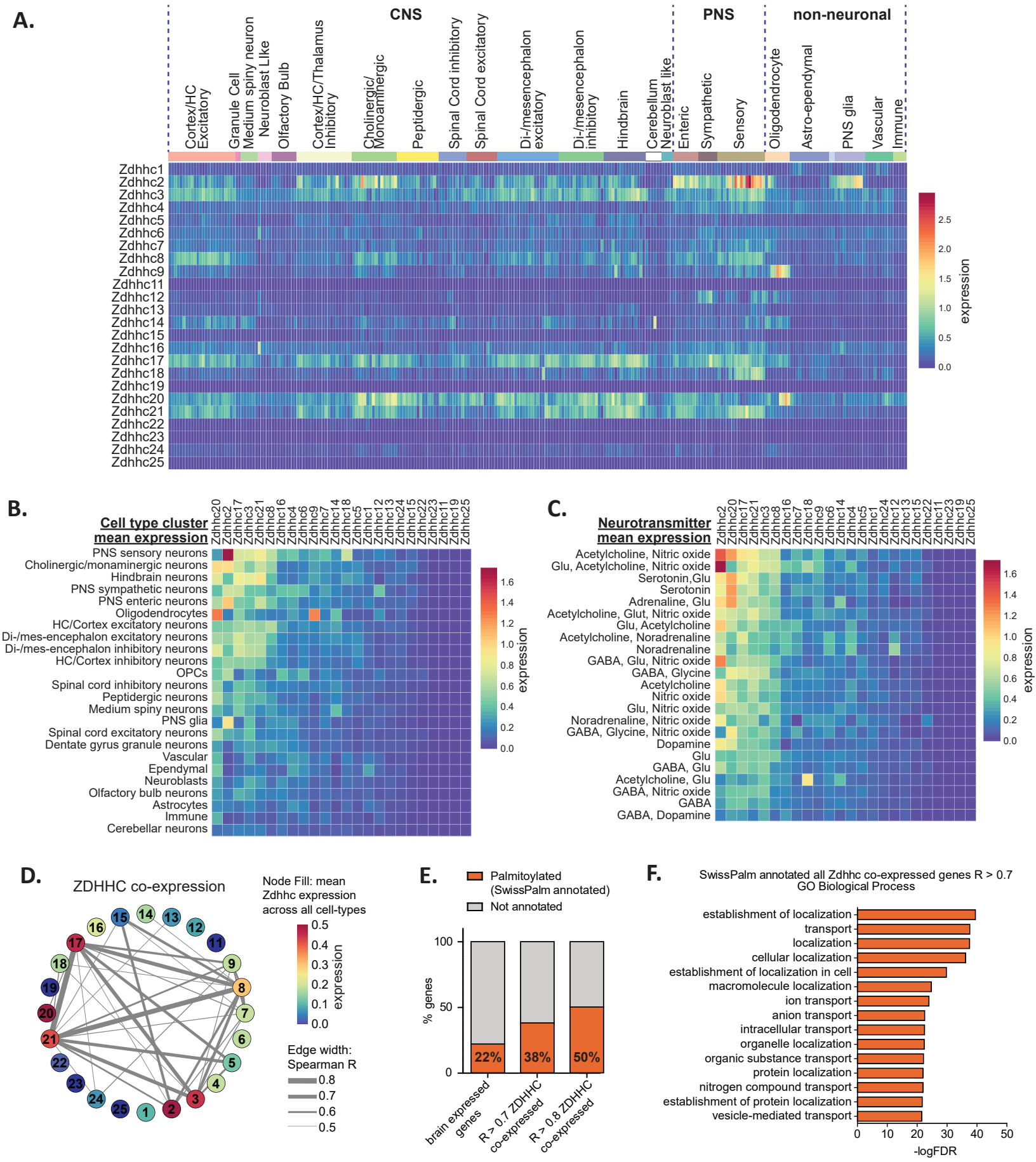
A.
CNS
PNS
non-neuronal
Cortex/HC Excitatory
Granule Cell
Medium spiny neuron
Neuroblast LIke
Olfactory Bulb
Cortex/HC/Thalamus Inhibitory
Cholinergic/ Monoaminergic
Peptidergic
Spinal Cord inhibitory
Spinal Cord excitatory
Di-/mesencephalon excitatory
Di-/mesencephalon inhibitory
Hindbrain
Cerebellum
Neuroblast like
Enteric
Sympathetic
Sensory
Oligodendrocyte
Astro-ependymal
PNS glia
Vascular
Immune
Zdhhc1
Zdhhc2
Zdhhc3
Zdhhc4
Zdhhc5
Zdhhc6
Zdhhc7
Zdhhc8
Zdhhc9
Zdhhc11
Zdhhc12
Zdhhc13
Zdhhc14
Zdhhc15
Zdhhc16
Zdhhc17
Zdhhc18
Zdhhc19
Zdhhc20
Zdhhc21
Zdhhc22
Zdhhc23
Zdhhc24
Zdhhc25
expression
B.
Cell type cluster mean expression
PNS sensory neurons
Cholinergic/monaminergic neurons
Hindbrain neurons
PNS sympathetic neurons
PNS enteric neurons
Oligodendrocytes
HC/Cortex excitatory neurons
Di-/mes-encephalon excitatory neurons
Di-/mes-encephalon inhibitory neurons
HC/Cortex inhibitory neurons
OPCs
Spinal cord inhibitory neurons
Peptidergic neurons
Medium spiny neurons
PNS glia
Spinal cord excitatory neurons
Dentate gyrus granule neurons
Vascular
Ependymal
Neuroblasts
Olfactory bulb neurons
Astrocytes
Immune
Cerebellar neurons
C.
Neurotransmitter mean expression
Acetylcholine, Nitric oxide
Glu, Acetylcholine, Nitric oxide
Serotonin,Glu
Serotonin
Adrenaline, Glu
Acetylcholine, Glut, Nitric oxide
Glu, Acetylcholine
Acetylcholine, Noradrenaline
Noradrenaline
GABA, Glu, Nitric oxide
GABA, Glycine
Acetylcholine
Nitric oxide
Glu, Nitric oxide
Noradrenaline, Nitric oxide
GABA, Glycine, Nitric oxide
Dopamine
Glu
GABA, Glu
Acetylcholine, Glu
GABA, Nitric oxide
GABA
GABA, Dopamine
D.
ZDHHC co-expression
Node Fill: mean Zdhhc expression across all cell-types
Edge width: Spearman R
E.
Palmitoylated (SwissPalm annotated)
Not annotated
% genes
22%
38%
50%
brain expressed genes
R > 0.7 ZDHHC co-expressed
R > 0.8 ZDHHC co-expressed
F.
SwissPalm annotated all Zdhhc co-expressed genes R > 0.7
GO Biological Process
establishment of localization
transport
localization
cellular localization
establishment of localization in cell
macromolecule localization
ion transport
anion transport
intracellular transport
organelle localization
organic substance transport
protein localization
nitrogen compound transport
establishment of protein localization
vesicle-mediated transport
-logFDR

Figure 2

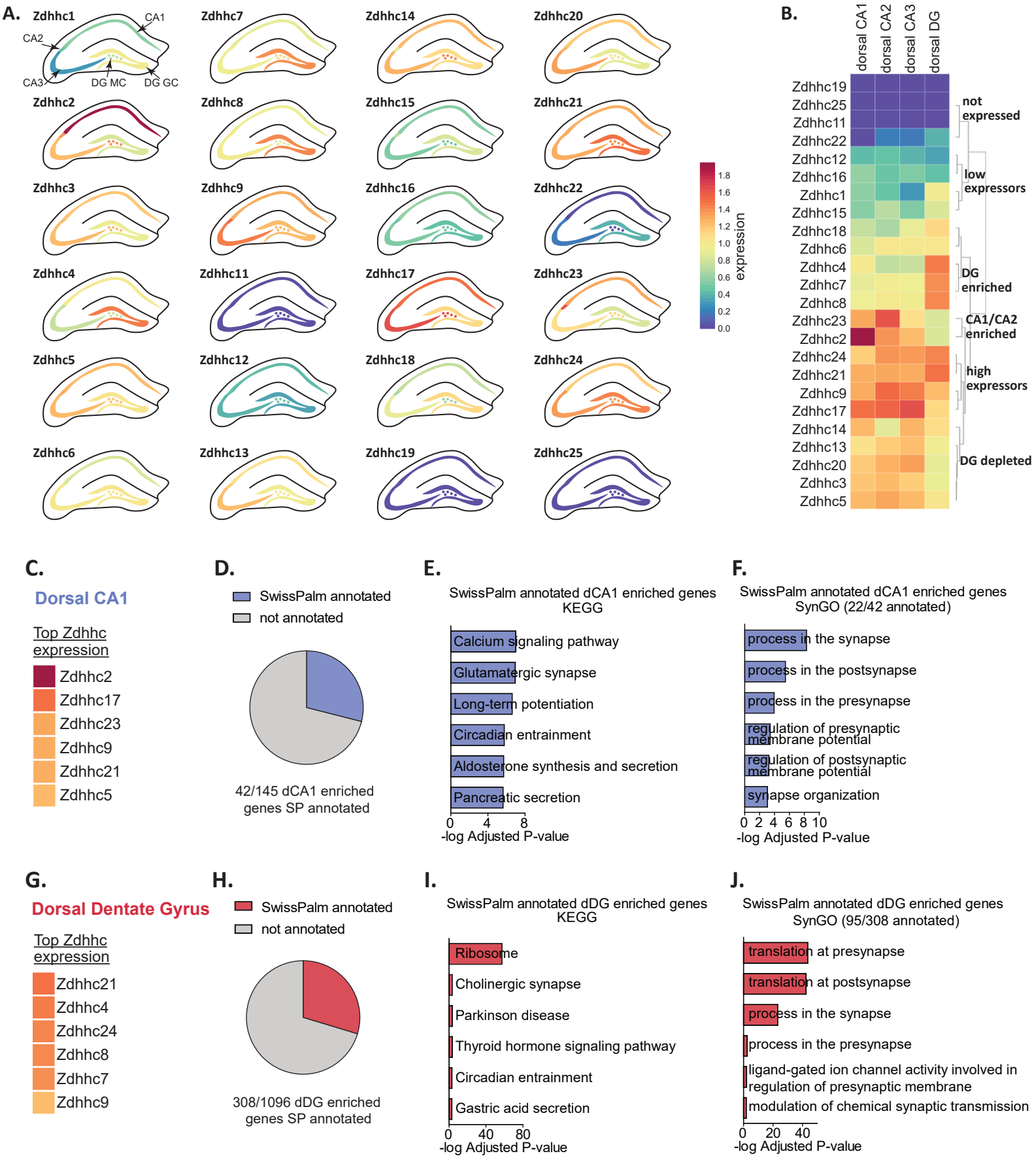
A.
Zdhhc1
CA1
CA2
CA3
DG MC
DG GC
Zdhhc2
Zdhhc3
Zdhhc4
Zdhhc5
Zdhhc6
Zdhhc7
Zdhhc8
Zdhhc9
Zdhhc11
Zdhhc12
Zdhhc13
Zdhhc14
Zdhhc15
Zdhhc16
Zdhhc17
Zdhhc18
Zdhhc19
Zdhhc20
Zdhhc21
Zdhhc22
Zdhhc23
Zdhhc24
Zdhhc25
expression
1.8
1.6
1.4
1.2
1.0
0.8
0.6
0.4
0.2
0.0
B.
dorsal CA1
dorsal CA2
dorsal CA3
dorsal DG
Zdhhc19
Zdhhc25
Zdhhc11
Zdhhc22
Zdhhc12
Zdhhc16
Zdhhc1
Zdhhc15
Zdhhc18
Zdhhc6
Zdhhc4
Zdhhc7
Zdhhc8
Zdhhc23
Zdhhc2
Zdhhc24
Zdhhc21
Zdhhc9
Zdhhc17
Zdhhc14
Zdhhc13
Zdhhc20
Zdhhc3
Zdhhc5
not expressed
low expressors
DG enriched
CA1/CA2 enriched
high expressors
DG depleted
C.
Dorsal CA1
Top Zdhhc expression
Zdhhc2
Zdhhc17
Zdhhc23
Zdhhc9
Zdhhc21
Zdhhc5
D.
SwissPalm annotated
not annotated
42/145 dCA1 enriched genes SP annotated
E.
SwissPalm annotated dCA1 enriched genes KEGG
Calcium signaling pathway
Glutamatergic synapse
Long-term potentiation
Circadian entrainment
Aldosterone synthesis and secretion
Pancreatic secretion
0
4
8
-log Adjusted P-value
F.
SwissPalm annotated dCA1 enriched genes SynGO (22/42 annotated)
process in the synapse
process in the postsynapse
process in the presynapse
regulation of presynaptic membrane potential
regulation of postsynaptic membrane potential
synapse organization
0 2 4 6 8 10
-log Adjusted P-value
G.
Dorsal Dentate Gyrus
Top Zdhhc expression
Zdhhc21
Zdhhc4
Zdhhc24
Zdhhc8
Zdhhc7
Zdhhc9
H.
SwissPalm annotated
not annotated
308/1096 dDG enriched genes SP annotated
I.
SwissPalm annotated dDG enriched genes KEGG
Ribosome
Cholinergic synapse
Parkinson disease
Thyroid hormone signaling pathway
Circadian entrainment
Gastric acid secretion
0
40
80
-log Adjusted P-value
J.
SwissPalm annotated dDG enriched genes SynGO (95/308 annotated)
translation at presynapse
translation at postsynapse
process in the synapse
process in the presynapse
ligand-gated ion channel activity involved in regulation of presynaptic membrane
modulation of chemical synaptic transmission
0
20
40
-log Adjusted P-value

Figure 3

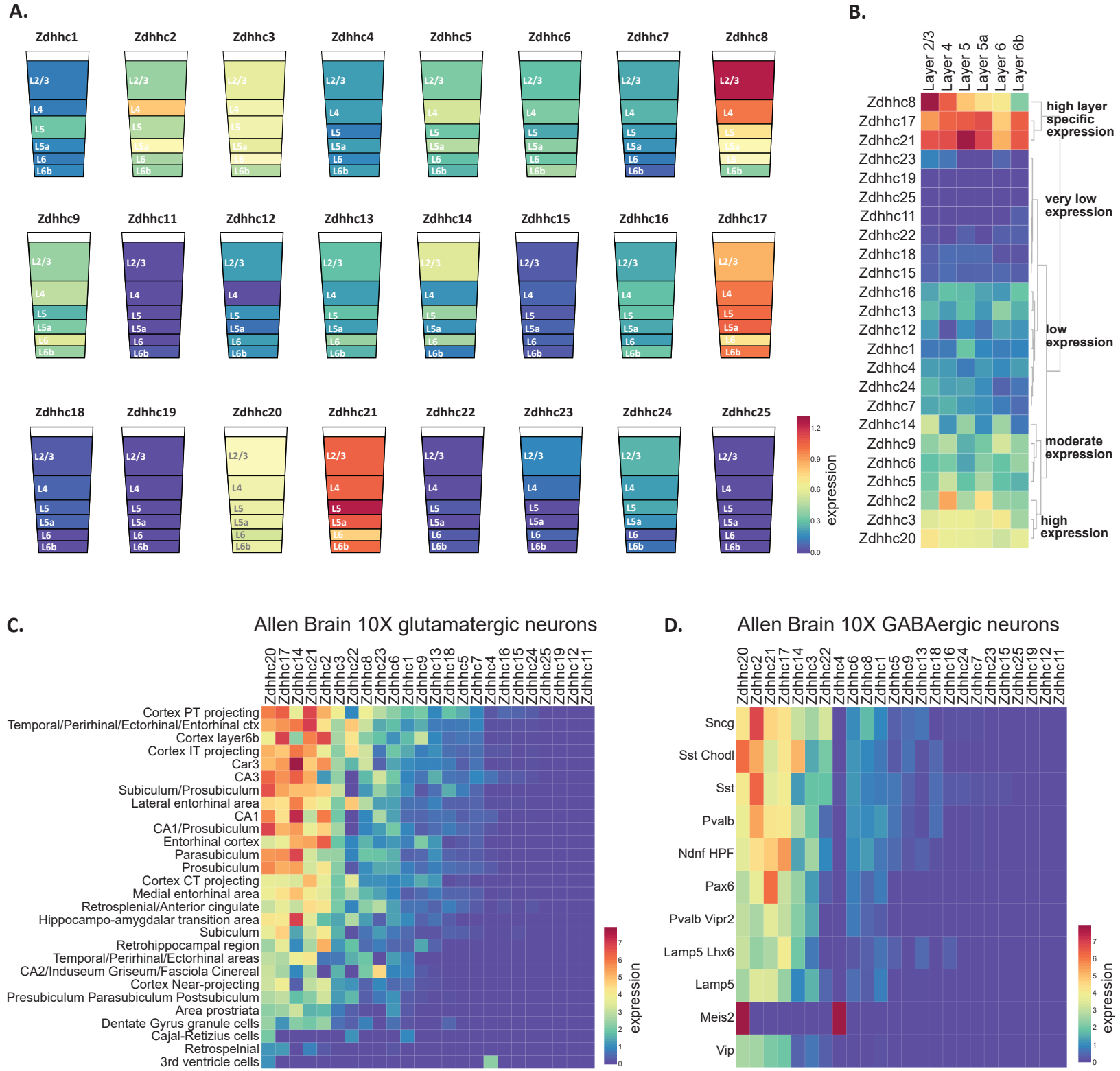
A.
Zdhhc1
Zdhhc2
Zdhhc3
Zdhhc4
Zdhhc5
Zdhhc6
Zdhhc7
Zdhhc8
Zdhhc9
Zdhhc11
Zdhhc12
Zdhhc13
Zdhhc14
Zdhhc15
Zdhhc16
Zdhhc17
Zdhhc18
Zdhhc19
Zdhhc20
Zdhhc21
Zdhhc22
Zdhhc23
Zdhhc24
Zdhhc25
L2/3
L4
L5
L5a
L6
L6b
expression
B.
Layer 2/3
Layer 4
Layer 5
Layer 5a
Layer 6
Layer 6b
high layer specific expression
very low expression
low expression
moderate expression
high expression
C.
Allen Brain 10X glutamatergic neurons
Cortex PT projecting
Temporal/Perirhinal/Ectorhinal/Entorhinal ctx
Cortex layer6b
Cortex IT projecting
Car3
CA3
Subiculum/Prosubiculum
Lateral entorhinal area
CA1
CA1/Prosubiculum
Entorhinal cortex
Parasubiculum
Prosubiculum
Cortex CT projecting
Medial entorhinal area
Retrosplenial/Anterior cingulate
Hippocampo-amygdalar transition area
Subiculum
Retrohippocampal region
Temporal/Perirhinal/Ectorhinal areas
CA2/Induseum Griseum/Fasciola Cinereal
Cortex Near-projecting
Presubiculum Parasubiculum Postsubiculum
Area prostriata
Dentate Gyrus granule cells
Cajal-Retizius cells
Retrospelnial
3rd ventricle cells
D.
Allen Brain 10X GABAergic neurons
Sncg
Sst Chodl
Sst
Pvalb
Ndnf HPF
Pax6
Pvalb Vipr2
Lamp5 Lhx6
Lamp5
Meis2
Vip

Figure 4

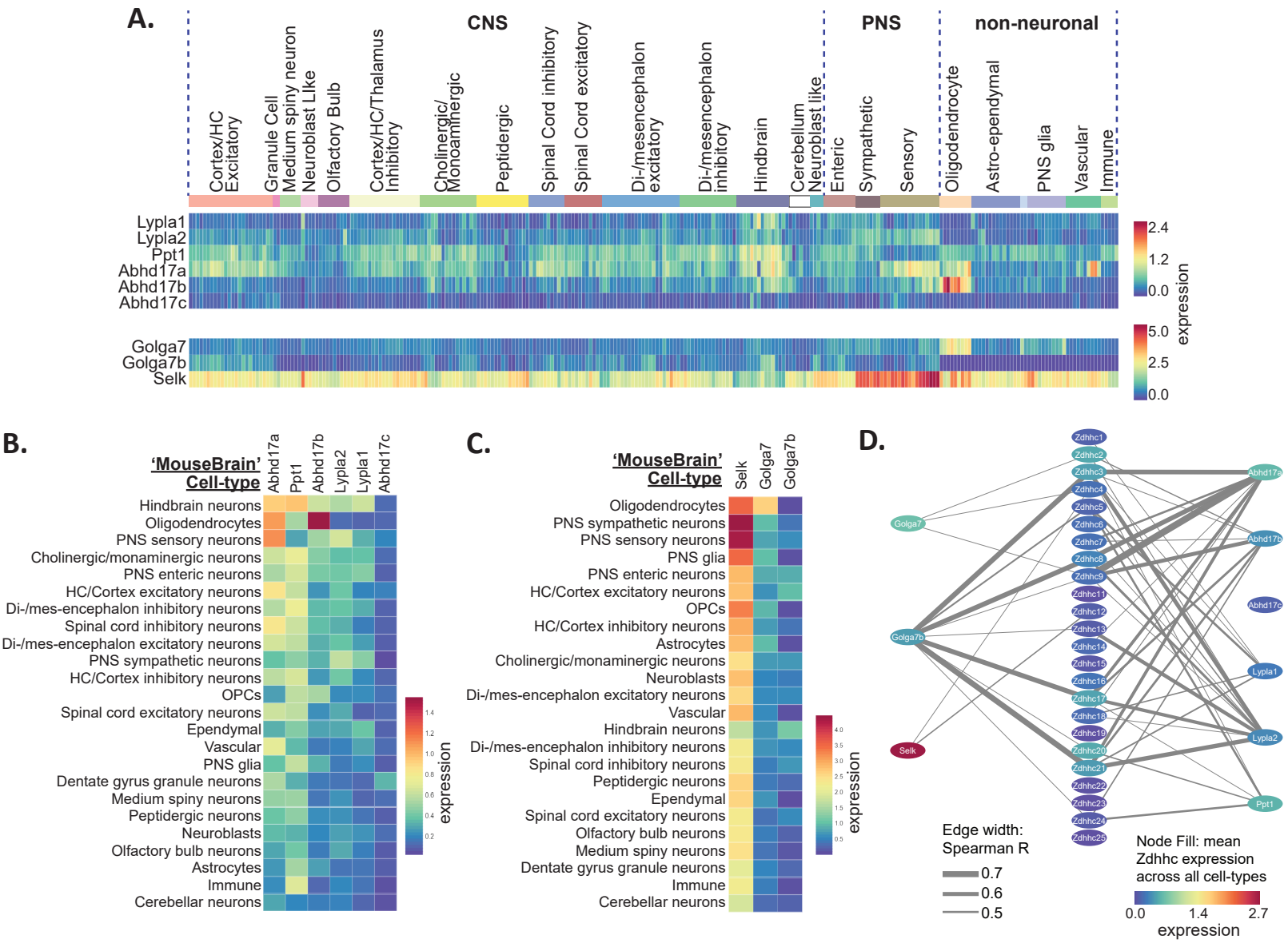
A.
CNS
PNS
non-neuronal
Cortex/HC Excitatory
Granule Cell
Medium spiny neuron
Neuroblast Like
Olfactory Bulb
Cortex/HC/Thalamus Inhibitory
Cholinergic/ Monoaminergic
Peptidergic
Spinal Cord inhibitory
Spinal Cord excitatory
Di-/mesencephalon excitatory
Di-/mesencephalon inhibitory
Hindbrain
Cerebellum
Neuroblast like
Enteric
Sympathetic
Sensory
Oligodendrocyte
Astro-ependymal
PNS glia
Vascular
Immune
Lypla1
Lypla2
Ppt1
Abhd17a
Abhd17b
Abhd17c
Golga7
Golga7b
Selk
2.4
1.2
0.0
expression
5.0
2.5
0.0
B.
'MouseBrain' Cell-type
Abhd17a
Ppt1
Abhd17b
Lypla2
Lypla1
Abhd17c
Hindbrain neurons
Oligodendrocytes
PNS sensory neurons
Cholinergic/monaminergic neurons
PNS enteric neurons
HC/Cortex excitatory neurons
Di-/mes-encephalon inhibitory neurons
Spinal cord inhibitory neurons
Di-/mes-encephalon excitatory neurons
PNS sympathetic neurons
HC/Cortex inhibitory neurons
OPCs
Spinal cord excitatory neurons
Ependymal
Vascular
PNS glia
Dentate gyrus granule neurons
Medium spiny neurons
Peptidergic neurons
Neuroblasts
Olfactory bulb neurons
Astrocytes
Immune
Cerebellar neurons
expression
C.
'MouseBrain' Cell-type
Selk
Golga7
Golga7b
Oligodendrocytes
PNS sympathetic neurons
PNS sensory neurons
PNS glia
PNS enteric neurons
HC/Cortex excitatory neurons
OPCs
HC/Cortex inhibitory neurons
Astrocytes
Cholinergic/monaminergic neurons
Neuroblasts
Di-/mes-encephalon excitatory neurons
Vascular
Hindbrain neurons
Di-/mes-encephalon inhibitory neurons
Spinal cord inhibitory neurons
Peptidergic neurons
Ependymal
Spinal cord excitatory neurons
Olfactory bulb neurons
Medium spiny neurons
Dentate gyrus granule neurons
Immune
Cerebellar neurons
expression
D.
Golga7
Golga7b
Selk
Zdhhc1
Zdhhc2
Zdhhc3
Zdhhc4
Zdhhc5
Zdhhc6
Zdhhc7
Zdhhc8
Zdhhc9
Zdhhc11
Zdhhc12
Zdhhc13
Zdhhc14
Zdhhc15
Zdhhc16
Zdhhc17
Zdhhc18
Zdhhc19
Zdhhc20
Zdhhc21
Zdhhc22
Zdhhc23
Zdhhc24
Zdhhc25
Abhd17a
Abhd17b
Abhd17c
Lypla1
Lypla2
Ppt1
Edge width: Spearman R
0.7
0.6
0.5
Node Fill: mean Zdhhc expression across all cell-types
0.0
1.4
2.7
expression

Figure 5

A. ***Zdhhc8*** **neonatal expression Rosenberg et al <P11**

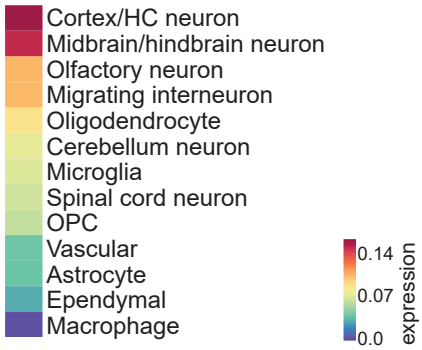

B. ***Zdhhc8*** **adolescent expression 'MouseBrain' P25**

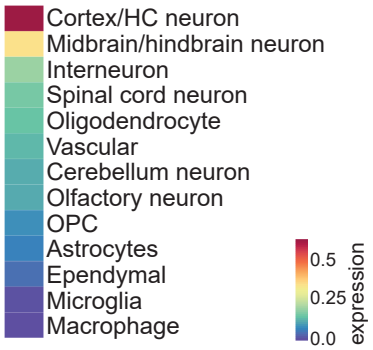

C. ***Zdhhc8*** **adult expression 'Protein Atlas' Mouse P60**

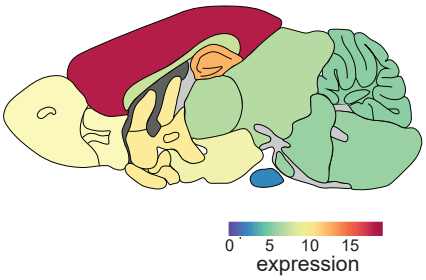

D. ***Zdhhc9*** **neonatal expression Rosenberg et al <P11**

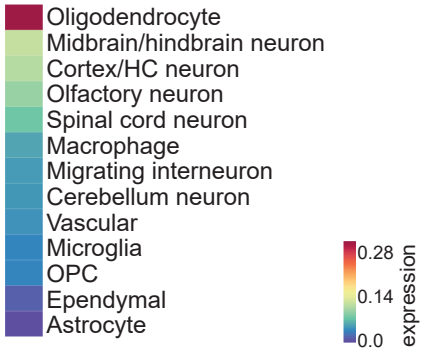

E. ***Zdhhc9*** **adolescent expression 'MouseBrain' P25**

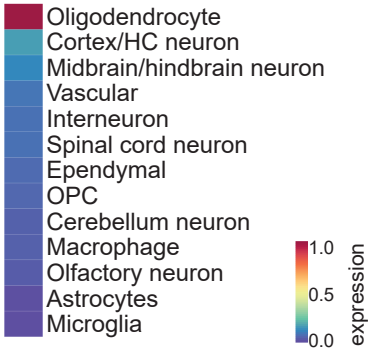

F. ***Zdhhc9*** **adult expression 'Protein Atlas' Mouse P60**

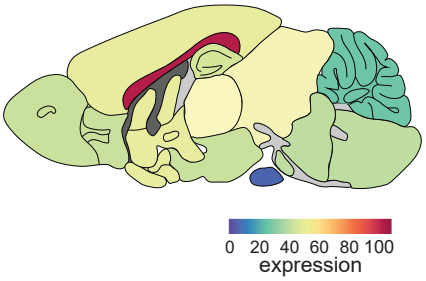

G. ***Ppt1*** **neonatal expression Rosenberg et al <P11**

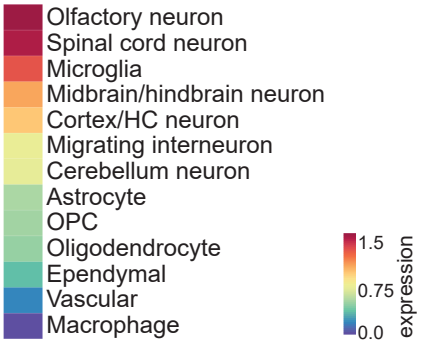

H. ***Ppt1*** **adolescent expression 'MouseBrain' P25**

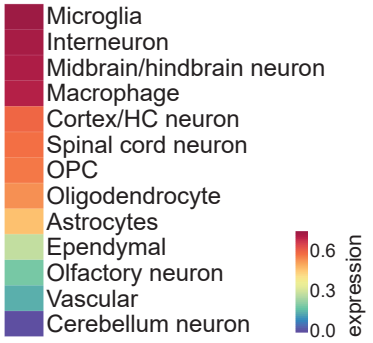

I. ***Ppt1*** **adult expression 'Protein Atlas' Mouse P60**

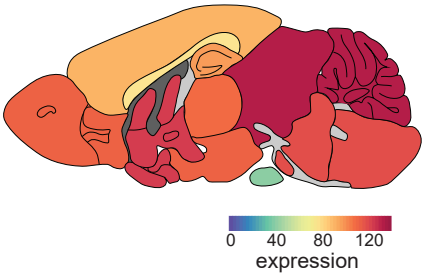

Figure 6

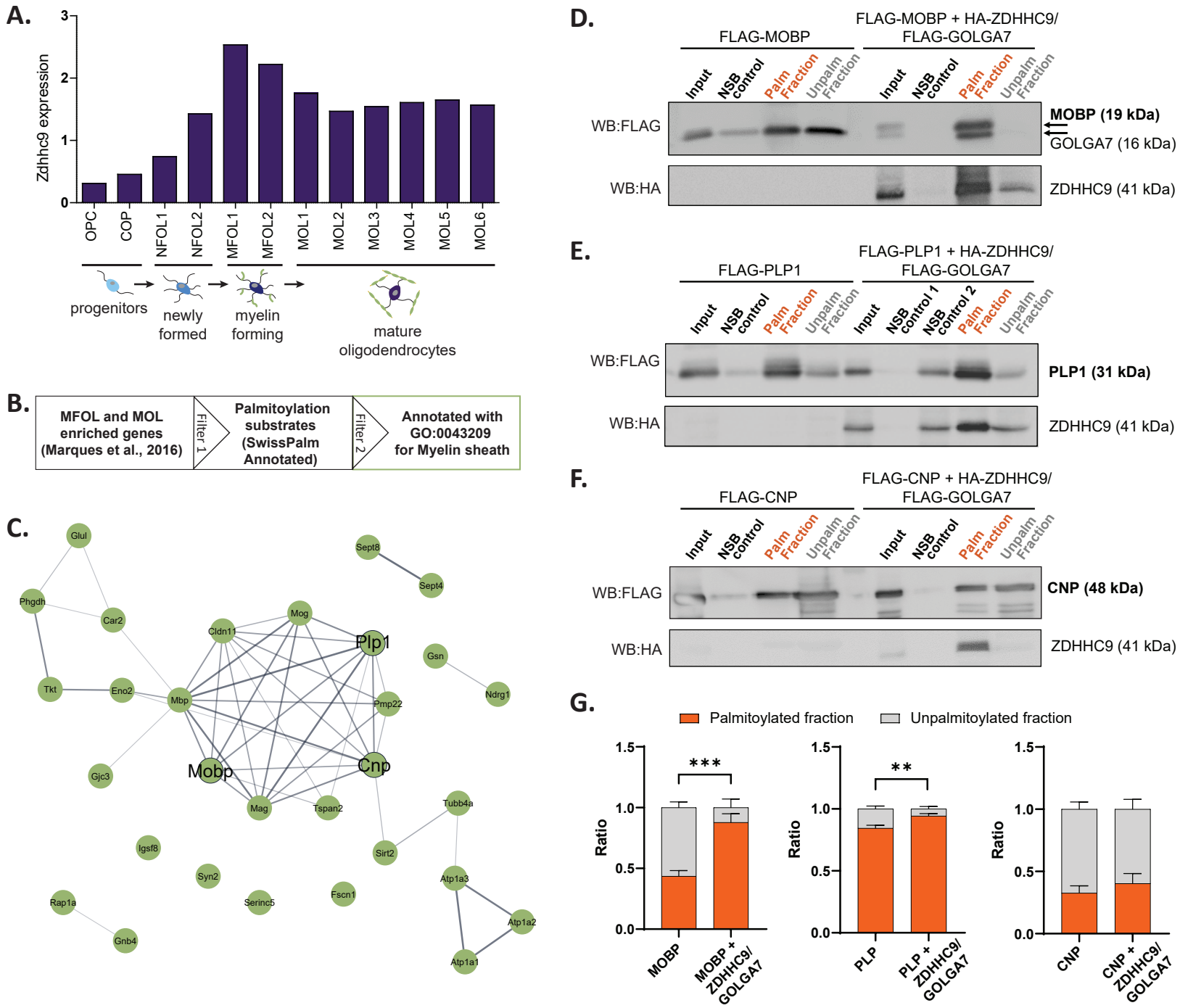
A.
Zdhhc9 expression
0
1
2
3
OPC
COP
NFOL1
NFOL2
MFOL1
MFOL2
MOL1
MOL2
MOL3
MOL4
MOL5
MOL6
progenitors
newly formed
myelin forming
mature oligodendrocytes
B.
MFOL and MOL enriched genes (Marques et al., 2016)
Filter 1
Palmitoylation substrates (SwissPalm Annotated)
Filter 2
Annotated with GO:0043209 for Myelin sheath
C.
Glul
Phgdh
Car2
Tkt
Eno2
Mbp
Gjc3
Mobp
Mag
Tspan2
Cldn11
Mog
Plp1
Pmp22
Cnp
Sept8
Sept4
Gsn
Ndrg1
Tubb4a
Sirt2
Atp1a3
Atp1a2
Atp1a1
Igsf8
Syn2
Rap1a
Gnb4
Serinc5
Fscn1
D.
FLAG-MOBP
FLAG-MOBP + HA-ZDHHC9/ FLAG-GOLGA7
Input
NSB control
Palm Fraction
Unpalm Fraction
WB:FLAG
WB:HA
MOBP (19 kDa)
GOLGA7 (16 kDa)
ZDHHC9 (41 kDa)
E.
FLAG-PLP1
FLAG-PLP1 + HA-ZDHHC9/ FLAG-GOLGA7
NSB control 1
NSB control 2
PLP1 (31 kDa)
F.
FLAG-CNP
FLAG-CNP + HA-ZDHHC9/ FLAG-GOLGA7
CNP (48 kDa)
G.
Palmitoylated fraction
Unpalmitoylated fraction
Ratio
***
**
MOBP
MOBP + ZDHHC9/ GOLGA7
PLP
PLP + ZDHHC9/ GOLGA7
CNP
CNP + ZDHHC9/ GOLGA7